JOURNAL OF PETROLOGY | VOLUME 39 | NUMBER 1 | PAGES 125–154 | 1998

Chemical and Isotopic Composition of Lavas from the Northern Mariana Trough: Implications for Magmagenesis in Back-arc Basins

ROBERT F. GRIBBLE[1], ROBERT J. STERN[1,*], SALLY NEWMAN[2], SHERMAN H. BLOOMER[3] AND TIM O'HEARN[4]

[1]CENTER FOR LITHOSPHERIC STUDIES, UNIVERSITY OF TEXAS AT DALLAS, RICHARDSON, TX 75083-0688, USA

[2]DIVISION OF GEOLOGICAL AND PLANETARY SCIENCE, CALIFORNIA INSTITUTE OF TECHNOLOGY, PASADENA, CA 91125, USA

[3]DEPARTMENT OF GEOSCIENCES, OREGON STATE UNIVERSITY, CORVALLIS, OR 97331, USA

[4]SMITHSONIAN INSTITUTION, WASHINGTON, DC 20560, USA

RECEIVED JANUARY 30, 1997; REVISED TYPESCRIPT ACCEPTED AUGUST 4, 1997

We report the results of a geochemical and isotopic study of mostly basaltic glasses recovered from 25 dredge stations along the northernmost 500 km of the Mariana Trough extension axis. The distribution of samples links regions of seafloor spreading to the south with regions farther north where a progression of rifting styles accompanies the earliest stages of back-arc basin extension. Petrographic, chemical and isotopic compositions of igneous rocks reflect the changing styles of extension, with typical back-arc basin basalts in the south which become increasingly similar to arc lavas to the north. Felsic lavas also appear along the extensional axis in the north. Glassy, sparsely phyric basalts characterize regions of seafloor spreading. Felsic lavas and porphyritic basalts occur in the northern, rifting portion. Geochemical and isotopic compositions distinguish between mature arc portions (Ce/Pb <10, Ba/La >20; $^{206}Pb/^{204}Pb$ >18·5, $^{87}Sr/^{86}Sr$ >0·7032, $\varepsilon_{Nd} < +8$) and regions of back-arc spreading (Ce/Pb >10, Ba/La <20; $^{206}Pb/^{204}Pb$ <18·9, $^{87}Sr/^{86}Sr$ <0·7032, $\varepsilon_{Nd} > +7$). Samples from along the extensional axis of the northern Mariana Trough show progressive changes in chemical and isotopic compositions, from back-arc basin basalts that formed by seafloor spreading northward through increasingly arc-like basalts, until lavas that are indistinguishable from arc lavas are encountered in the northernmost portion of the rift. Batch-melting models indicate that northernmost rift lavas reflect higher degrees of melting, with 13 ± 5% melting where seafloor spreading occurs, doubling to 28 ± 8% for the northernmost part of the rift axis. The greater degree of melting in the north reflects the greater amount of water added to the mantle source, reflecting the arc-like nature of the source region and melt generation style characteristic of the initial stages of back-arc basin formation. Our data indicate that $F = 0{\cdot}44W + 0{\cdot}07$, *where* F *is the degree of mantle melting and* W *is the percent water in the mantle. 'True' back-arc basin basalts are generated by adiabatic decompression associated with mantle upwelling in mature extensional settings. Eruption of 'true' back-arc basin basalts accompanies seafloor spreading, which begins when the basin is 100–150 km wide. The arc is disrupted during early rift formation, because arc magmatism is captured by the extension axis, but the generation of arc melts by hydrous melting of the mantle wedge continues whether or not back-arc extension is occurring. Back-arc basin seafloor spreading requires development of an upwelling mantle flow regime, allowing melting by adiabatic decompression, similar to that responsible for mid-ocean ridge basalt (MORB). The arc begins to re-form once extension progresses nearly to the point of seafloor spreading.*

KEY WORDS: *arc magmas; back-arc basin basalt; isotope geochemistry; Mariana Islands; trace elements*

*Corresponding author.

INTRODUCTION

Back-arc basins (BAB) such as the Mariana Trough form by rifting of active magmatic arcs (Karig, 1971). We define mature BAB to be those where extension is principally accomplished by seafloor spreading. Our understanding of mature BAB has benefited because the model of melting as a result of adiabatic upwelling developed for mid-ocean ridges (e.g. Forsyth, 1992) is directly applicable. Among the differences between mid-ocean ridge (MOR) and BAB spreading is that the latter may reflect lower mantle temperatures, that asymmetric spreading may be the norm, and that the mantle is hydrated and metasomatized by a 'subduction component' that is ultimately derived from the subducted lithosphere and sediments.

Our understanding of the early stage in BAB opening—defined as the interval between initial rifting and the onset of seafloor spreading—is less advanced than our understanding of the mechanical and chemical dynamics of mature back-arc basins. This is largely because we do not yet understand how the transition is accomplished from arc magmagenetic and tectonic processes to those of seafloor spreading as the extension continues. Continental rifting leading to MOR seafloor spreading offers few insights: continental rifting is often amagmatic whereas arc rifting is characteristically preceded, accompanied, and followed by vigorous volcanism. Large volumes of mafic igneous rocks may be generated at the close of continental rifting, just before development of seafloor spreading (White & McKenzie, 1989); nothing like this has been proposed for corresponding stages in the development of back-arc basins.

We have two firm constraints regarding the changing style of magmagenesis during early BAB opening: (1) before opening begins, dominant magmagenetic processes and sources are those causing the point-source igneous style characteristic of arcs; and (2) after the early stage of opening is over, seafloor spreading processes and sources dominate. Early BAB evolution occurs as the transition from (1) to (2) is accomplished. This study uses early BAB lavas to better understand this transition.

There are two outstanding controversies which, if resolved, would illuminate problems of early BAB development. The first controversy concerns whether or not arc volcanism ceases during BAB extension. Crawford *et al.* (1981) argued that magmatic activity for arc–BAB pairs, especially in the Western Pacific region, is asynchronous, with little arc volcanism while the back-arc basin is growing. If true, this requires strong coupling between arc and BAB magmatic systems, with clear implications for our understanding of convergent margin magmatic systems. This model has been questioned, and more recent interpretations call for synchronous BAB and arc magmatism to reflect the first and second stages of melt depletion in a convecting mantle wedge (McCulloch & Gamble, 1991).

The second controversy concerns the nature of early BAB magmas, with some scientists calling for a progressive evolution from arc-like to more mid-ocean ridge basalt (MORB)-like basaltic compositions (e.g. Stern *et al.*, 1990), whereas others conclude that there are distinct basalt compositions erupted in all stages of BAB development. The latter group infers that early BAB lavas have compositions distinct from arc tholeiites and indistinguishable from back-arc basin basalt (BABB) from the time of rift initiation (e.g. Fryer *et al.*, 1990). Understanding whether or not basalt compositions change with rifting and, if so, how, is critical for understanding convergent margin dynamics. For example, if BAB seafloor spreading reflects induced upwelling and decompression melting of the mantle (e.g. Gribble *et al.*, 1996), then analogy with continental rifting progressing to seafloor spreading indicates that a large degree of extension ($\beta \sim 5$; White & McKenzie, 1989) (where β specifies the amount of extension in a rift, and equals the width ratio of extended crust to that of the same crustal tract prior to extension) is necessary before there is sufficient mantle upwelling to generate BABB. If, on the other hand, BABB erupt from the beginning stages of extension, magmagenesis may not be a direct manifestation of mantle upwelling induced by extension. This would tend to support active rift models calling for injection of asthenospheric material to force BAB rifting (e.g. Tatsumi *et al.*, 1989).

A related issue concerns the increasingly common recognition that felsic lavas erupt during early BAB formation (Clift, 1995; Marsaglia, 1995). Together with basalts, these form a bimodal suite that accompanies the early stages of BAB formation. Eruption of dacitic lavas appears to be a feature that distinguishes early BAB rifting from BAB spreading, but we do not yet understand the genesis of BAB felsic magmas. Those concerned with this problem are split between advocates of fractionation of mafic magma and advocates for anatexis of amphibolite-facies mafic crust (Beard, 1995). Furthermore, felsic bodies interpreted to have formed in ancient back-arc basin settings host important ore deposits on land (Kuroko-type massive sulphides). This provides an economic rationale for studies of early BAB magmatic and tectonic activity.

This paper presents new major, trace element, and radiogenic isotope data for fresh lavas erupted along the extension axis in the northern Mariana Trough back-arc basin between 23°N and 18°45′N (Fig. 1c). Geophysical studies indicate that rifting has propagated through this region and that this section of the Mariana Trough extension axis provides a complete evolutionary sequence of back-arc basin development. In this paper we take

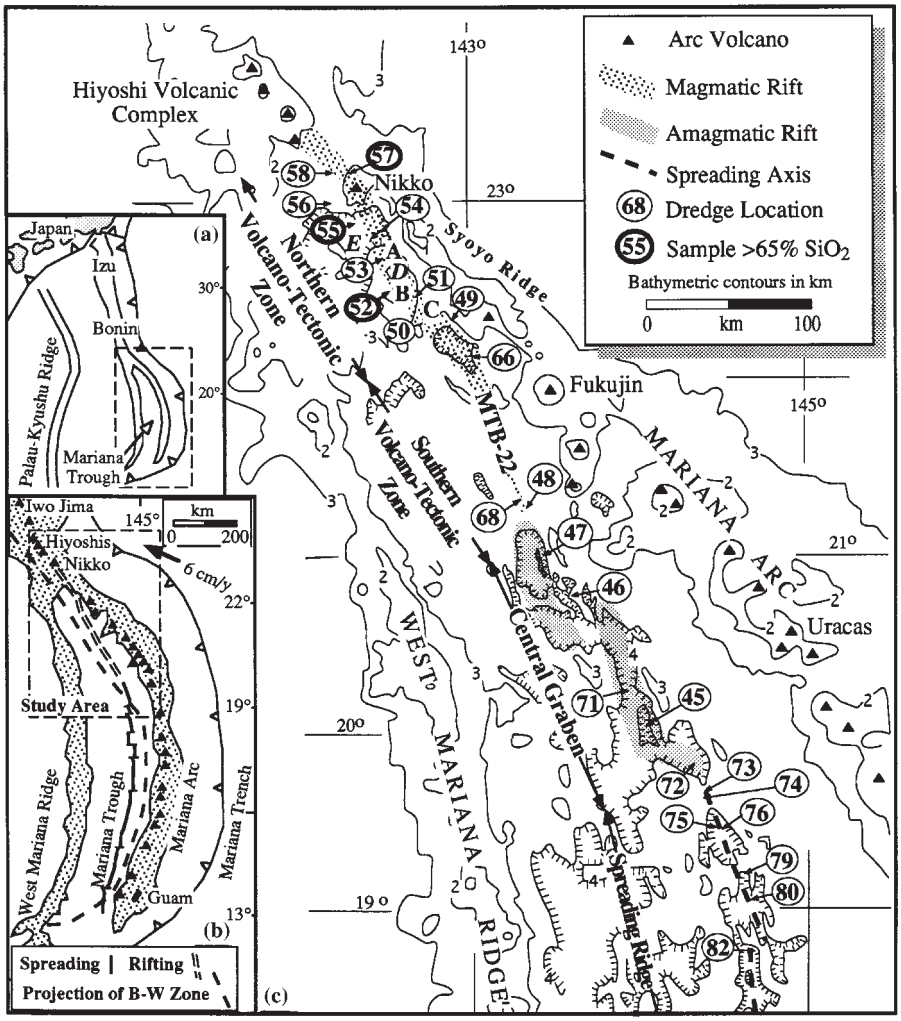

Fig. 1. Location map of the northern Mariana Trough. (a) Location of the Mariana Arc system in the western Pacific. (b) Location of the study area (dashed rectangle) within the Mariana Arc system. Different styles of extension are indicated, with seafloor spreading in the southern and central portions and rifting in the northern portion of the Trough. It should also be noted that the surface projection of westernmost extent of the Benioff–Wadati Zone is indicated (Projection of B-W Zone), after Eguchi (1984). (c) Details of the study area in the northern Mariana Trough. Circled numbers locate successful dredges during TUNES Leg 7. The extension axis is shown by patterns that reflect regions with different tectonic styles. ▲, active (or dormant) Mariana Arc volcanoes. Samples from region labeled MTB-22 were studied by Stern *et al.* (1990). The capital letters A, B and C identify large seamounts along the extension axis in the northern Mariana Trough (Martinez *et al.*, 1995). Locations of samples studied by Jackson (1989) are shown with italicized capital letters *D* and *E*. Dredge locations KH84-1-23 and -24 (Shibata & Segawa, 1985) are not shown but are near dredge 45.

advantage of this opportunity to understand the relationship between BAB tectonic evolution and magmagenesis, from the time of rift initiation through development of seafloor spreading.

GEOLOGIC SETTING AND PREVIOUS WORK

The Mariana Arc system is the southern half of the 2500 km long intra-oceanic convergent margin extending from Japan south to Guam (Fig. 1a). Within this system, the Mariana Trough (MT) is an actively extending back-arc basin behind (west of) the Mariana Arc, with seafloor spreading in the southern two-thirds and rifting in the northern third (Figs 1b and 2). Though the MT floor at 18°N and to the south is, on average, >800 m deeper than the global mean for oceanic crust of similar age (Fig. 2; Park *et al.*, 1990), it is underlain by normal oceanic crust (Bibee *et al.*, 1980). The range of spreading rates at 18°N (half-rates 15–22 mm/year: Bibee *et al.*, 1980; Hussong & Uyeda, 1981) classifies it as a slowly spreading mid-ocean ridge (Malinverno, 1993). The extension axis is everywhere displaced away from the center of the

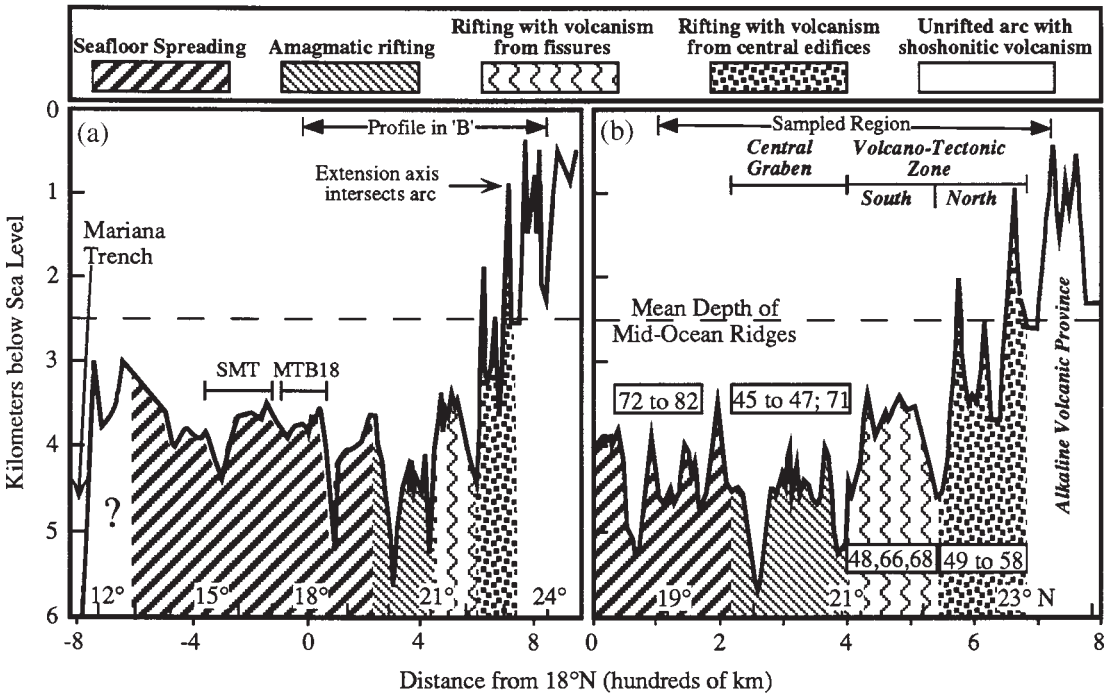

Fig. 2. Bathymetric and tectonic profiles along strike of the Mariana Trough. (a) Profile for the entire Trough, showing the changes in style of extension along the extension axis, and the segments of the spreading ridge previously studied: SMT, southern Mariana Trough studied by Gribble *et al.* (1996); MTB-18, ridge around 18°N studied by numerous investigators, including ALVIN diving and drilling during DSDP Leg 60. The typical depths of 3·5 km or deeper for the spreading ridge segment should be noted. The '?' in the extreme south indicates that the manner in which extension is accomplished in this region is poorly understood. (b) Northern Mariana Trough, the topic of this study. Changes in style of extension are indicated by province name (Central Graben, Volcano-Tectonic Zone) or by inferred process (pattern). Numbers in rectangles refer to TUNES 7 dredge numbers for each province.

basin and toward the arc; between 18° and 19°N, the spreading axis is ~100 km west of the active arc and about ~150 km east of the remnant arc. This asymmetry may either be due to a ridge jump (Bibee *et al.*, 1980), or because mechanically extended lithosphere underlies the western portion of the basin (Martinez *et al.*, 1995; Baker *et al.*, 1996). The extension axis in the northern Mariana Trough (NMT), progressively approaches the arc and finally intersects it at Nikko seamount (Fig. 1c). The Benioff–Wadati zone plunges vertically just west of the arc at 18°N (Katsumata & Sykes, 1969), and the spreading axis at this latitude is located 40–60 km west of its westernmost surface projection (Fig. 1b).

Igneous activity in arcs and back-arc basins is similar in some respects, although arc crustal growth is dominated by thickening because of lava accumulation and magmatic underplating and intrusion, whereas mature back-arc basin crustal growth occurs by seafloor spreading (Hawkins *et al.*, 1984). Volcanoes of the Mariana Arc show a range of sizes that reflect the evolution of the Trough. At 18°N, where the Trough is widest and seafloor spreading occurs, subaerial arc volcanoes that rise as much as 1 km above sea-level are common (Bloomer *et al.*, 1989*b*). As the crescent-shaped Mariana Trough narrows to the north and south, associated arc volcanoes become smaller; thus the Central Island Province of the Mariana Arc lies adjacent to the widest part of the Mariana Trough, whereas the Southern Seamount Province and Northern Seamount Province lie on the flanks of narrower Mariana Trough segments. The strong relationship between back-arc basin width and arc volcano size is interpreted to reflect the time since back-arc basin rifting began. Karig (1971) first suggested that back-arc basin rifting terminated arc volcanism, and our results agree with this interpretation, and show how this disruption occurs. The simplest explanation for the back-arc basin width–arc volcano size relationship is that bigger volcanoes are built adjacent to the most anciently rifted back-arc basin segments, and the smallest volcanoes are built adjacent to the most recently rifted back-arc basin segments. Another point that needs to be emphasized is that if back-arc basin is sufficiently mature that seafloor spreading is occurring, then arc and back-arc basin magmatism is compositionally and spatially distinct. On the other hand, if the back-arc basin is still rifting then it may be very difficult to resolve arc and back-arc basin volcanism, either on a spatial or compositional basis.

Recent geophysical surveys in the northern Mariana Trough provide a tectonic framework for petrologic studies. Martinez *et al.* (1995) divided the extension axis into four sections (Figs 1 and 2): (1) 23·1–22·1°N—the northern volcano-tectonic zone (NVTZ), characterized by asymmetric rifting accompanied by fissure eruption along normal faults and point source volcanism; (2) 22·1–21°N—the southern VTZ (SVTZ), characterized by localization of volcanic and tectonic activity and southward-progressive separation of the extension axis from the arc; (3) 21–19·7°N—the Central Graben, deeps produced by mechanical extension that expose BAB lower crust and upper mantle (Stern *et al.*, 1996); (4) south of 19·7°N at least as far south as 15°N extension happens by slow seafloor spreading as previously documented for the Mariana Trough near 18°N. Rifting occurs in sections 1, 2, and 3; we refer to lavas from these segments as 'Rift BABB', although some of these lavas are felsic. The gross bathymetric features that define the zone of seafloor spreading converge near the northern limit of spreading where the seafloor drops into a broad depression leading to the Central Graben (Martinez *et al.*, 1995). This also corresponds to the northernmost extent of gravimetric evidence for focused mantle upwelling beneath the trough axis (Martinez *et al.*, 1995).

The spreading ridge that we sampled in this study (19·7–18·8°N) is similar in axial depth and morphology to the trough axis farther south. Basalts from 19·7° to 18·8°N are referred to as 'Spreading Ridge' and are compositionally indistinguishable from samples recovered from other places in the Mariana Trough where seafloor spreading occurs; this includes basalts from the spreading axis near 18°N (MTB-18) and basalts from the spreading axis between 15° and 17°N (SMT) studied by Gribble *et al.* (1996). To emphasize the integrity of samples from the spreading ridge segment studied here with basalts from along the axis of seafloor spreading farther south, samples from all three segments—Spreading Ridge, MTB-18, and SMT—are grouped as Spread BABB. Mariana Trough Spread BABB differ only in detail, whereas we will show that Spread BABB and Rift BABB are strikingly different. We emphasize that compositional and isotopic differences between Spread BABB and Rift BABB reflect fundamental differences in the style of extension and the proximity of the extension axis to the locus of arc volcanism. Furthermore, because both rifting and spreading axes propagate northwards, these four sections (plus precursor shoshonitic volcanism north of Nikko) approximate the tectonic and petrologic evolution expected for the general evolution of the Mariana Trough. That is, processes now occurring at different places along the extension axis reveal the sequence of events leading to the formation of a back-arc basin.

We have a good understanding of Mariana Trough Spread BABB. Trace element and Sr isotopic data for Spread BABB are similar to MORB (Hart *et al.*, 1972). Pb isotopic studies also indicate a mantle source distinct from the source supplying Mariana Arc lavas (Meijer, 1976). Mariana Trough basalts nevertheless can generally be distinguished from true MORB by higher Al_2O_3/MgO, lower FeO*/MgO (Sinton & Fryer, 1987) and high H_2O (Garcia *et al.*, 1979; Stolper & Newman, 1994). In addition, when normalized to high field strength element (HFSE) abundances, the large ion lithophile element (LILE) and light rare earth element (LREE) abundances of relatively primitive Mariana Trough tholeiites are more than twice those of N-MORB (Fryer *et al.*, 1981; Wood *et al.*, 1981; Hawkins & Melchior, 1985). Based on the observation of similar basalts in other back-arc basins, Fryer *et al.* (1981) recognized back-arc basin basalts (BABB) as a rock type distinct from MORB.

More recent studies extend the range of compositions sampled in the Mariana Trough. Glasses very similar to arc tholeiites with respect to trace element and isotopic compositions are known from the MTB-18 suite (Hawkins *et al.*, 1990; Volpe *et al.*, 1990). The MORB source at 18°N is isotopically like Indian Ocean mantle (Volpe *et al.*, 1990; Hickey-Vargas, 1991). Gribble *et al.* (1996) identified two segments of spreading BAB in the SMT, with contrasting mean axial depths and basalt compositions. The northern segment is shallower than the southern segment and includes basalts with >2 wt % water and LILE/REE and isotopic ratios approaching Mariana Arc values. Basalts recovered from the southernmost SMT are indistinguishable from N-MORB, and basalts from the southern segment are characterized by low water and LILE concentrations and an isotopic signature very similar to that of Indian Ocean MORB.

The NMT was previously sampled within the SVTZ near 22°N (MTB-22 in Fig. 1c; Stern *et al.*, 1990), in the NVTZ at 22°39′N (volcanic cone, 'D' in Fig. 1c) and 22°48′N (fissure eruption, 'E' in Fig. 1c; KK01 and KK02, respectively, Jackson, 1989) and in the Central Graben [as summarized by Stern *et al.* (1996)]. These samples are predominantly tholeiitic and include high-MgO basalts (KK01, Jackson, 1989; KH84-1-24, Shibata & Segawa, 1985) and basalts with major element compositions similar to those from 18°N. Basalts collected near 22°N (MTB-22, Fig. 1c) in the southern VTZ have chemical and isotopic affinities with arc basalts (Stern *et al.*, 1990).

SAMPLE LOCATIONS AND PETROGRAPHY

Sampling was carried out in December 1991 aboard the R.V. *Thomas Washington* during Leg 7 of the TUNES expedition. This paper is based on samples recovered

Table 1: TUNES 7 dredge locations (arranged from north to south)

Dredge no.	Latitude (°N)	Longitude (°E)	Depth range (m)	Description of site; haul (in kg)
57	23·16	142·30	1565–1630	Horst N of Nikko (mag. hi); 200
58	23·15	142·12	1430–1580	Volc. cone W of Nikko; 15
56	23·00	142·17	1720–2630	Volc. cone WSW of Nikko; 100
55	22·87	142·32	3125–3205	Small ridge S of Nikko; 25
54	22·79	142·42	3430–3460	Ridge on NW flank of Smt. A; 30
53	22·69	142·45	1515–1790	Summit of Smt. A; 100
52	22·50	142·51	2090–2415	Parasitic cone on Smt. B; 75
51	22·49	142·67	1530–1640	Slope of basin SE of Smt. B; 100
50	22·38	142·79	2425–2760	SE side of Smt. C; 175
49	22·35	142·91	2240–3035	NE side of basin SE of Smt. C; 400
66	22·12	143·04	3105–3705	NE end SVTZ (N of MTB-22); 200
68	21·35	143·28	3800–3900	SE end SVTZ (S of MTB-22); 500
48	21·31	143·36	2860–2900	10 km ESE of Dredge 68; 1000
47	20·97	143·44	3680–5100	N-most deep in Central Graben; 400
46	20·82	143·55	3700–3700	Central Graben; 200
71	20·31	143·93	4300–4430	Central Graben; 200
45	20·04	144·07	4800–5175	S-most deep in Central Graben; 300
72	19·83	144·3	4450–4380	Cone in basin at N end of SR; 100
73	19·73	144·4	3600–4035	High on E side of SR; 1000
74	19·67	144·39	3630–3690	Axial high in SR rift; 50
76	19·45	144·54	3365–4480	Scarp on E side of SR; 20;
75	19·44	144·48	4380–4450	Axial ridge in SR rift axis; 2
79	19·19	144·61	3520–3900	?SR axis; 35
80	19·12	144·67	4040–4050	Small volcano in SR; 15
82	18·75	144·66	4300–4340	Ridge offset volcano; 400

SR, spreading ridge.

from 25 of these dredge lowerings. Twenty dredges recovered glass that we were able to separate and analyze, and four additional dredges included fresh samples that were analyzed as whole-rock powders. Dredge locations are listed in Table 1 and shown in Fig. 1. Petrographic features of the analyzed samples are presented in Table 2. Dredge collections were classified onboard according to petrographic features visible in hand specimen or under the binocular microscope—typically the type and amount of phenocrysts. Glass recovery in northern VTZ dredges was rare compared with the southern VTZ and further south. Vesicles and phenocrysts together commonly make up more than a third of the volume of VTZ samples. Vesicles and phenocrysts are present in subequal amounts and typically make up less than a third of the volume of lavas sampled south of the VTZ. Phenocryst assemblages are commonly ol + plag $\pm$ cpx. Clinopyroxene is common as a phenocryst in VTZ lavas, in contrast to its scarcity in samples recovered from the Central Graben south to the spreading BAB at 18°N and virtual absence south of 18°N. In the NMT, spinel is most common in VTZ lavas, where it forms large euhedra in olivine and, less commonly, in plagioclase.

SAMPLE PREPARATION AND ANALYSIS

Eighty glasses were analyzed by electron microprobe (EMP) at the Smithsonian Institute. EMP analytical procedures have been described by Melson *et al.* (1976). The complete data set is available from T. O'Hearn by e-mail <MNHMS002@SIVM.SI.EDU> or on disk as an ASCII file or in Microsoft Excel format. Major element analyses of the samples selected for isotope and trace element analysis at UT Dallas are given in Table 3. Two glass samples (D66:3-4 and D58:1-2) were analyzed by EMP at UT Dallas (Jongman Lee, analyst). Eleven

Table 2: Petrographic descriptions of analyzed samples (arranged from north to south)

Sample	% Vesicles	% OL	% PL	% CPX	Other
57:1-4	12	0	25	2	WR
57z	0	0	0	0	Glass chip
58:1-3	35	20	5	30	Interstitial glass
56:2-5	45	20–25	5–10	tr	CPX + OL glom; WR
55:1-1	5	5	0	tr	PL + CPX microphenos
54:1-1	40	3	4	1	skeletal OL
53:1-1	10	<1	24	1	WR
52:1-1	5–10	0	3–4	0	1–2% hornblende
51:1-1	40	3	10	tr	
50:1-5	<5	0	3	0	WR
49:1-1	12	0	25	1	WR
66:3-4	10	2	17	1	
68:1-2	20	2	6	2	
48:1-2,3	25	4	1	3	Spinel inclusions in OL
48:3-1	30	8	1	6	Spinel inclusions in OL
47:1-5	20	6	0	0	Spinel inclusions in OL
46:1-6	10	1	1	0	Spinel inclusions in OL
46:1-8	<2	5	tr	0	Spinel inclusions in OL
71:1-14	15	5	8	2	
45-5-2	tr	tr	tr	0	WR
72:2	4	4	0	0	
73:1-1	4	2	0	0	
73:2-1	4	2	0	0	
74:1-1	<2	9	2	0	Spinel in PL & OL
76:1-1	tr	tr	0	0	
75:1-2	tr	2	0	0	skeletal OL
79:1-1	5–10	<1	1–2	0	
80:1-3	<2	1–2	2–3	0	Spinel euhedra
82:1-1	5–10	3–4	1	0	Spinel euhedra

OL, olivine phenocrysts; PL, plagioclase phenocrysts; CPX, clinopyroxene phenocrysts; WR, analyzed as whole-rock powder, all others analyses performed on glass separates; glom, glomerocryst.

whole-rock powders selected from nine dredges were analyzed by X-ray fluorescence (XRF) at the University of Oklahoma (M. G. Abdelsalam, analyst). *mg*-number is calculated as $100(Mg/Mg + Fe^{2+})$, with Fe^{3+}/Fe^{2+} calculated by the algorithm of Kress & Carmichael (1988).

For a subset of 13 samples, H_2O and CO_2 were determined at Cal Tech by Fourier transform IR spectroscopic analysis of glass, following the general methods of Dixon *et al.* (1991) and modified by the use of a NicPlan microscope. Each sample was analyzed four times, using 1024–4096 scans and the redundant aperturing system set to 115 mm × 115 mm. Sample thicknesses ranged from 40 to 218 μm.

From the 25 successful dredges along the extension axis, 24 glasses and six whole-rock powders were selected for trace element and isotopic analyses. Glasses were processed first by picking + 20 mesh chips with minimal surface alteration. The chips were then crushed and cleaned ultrasonically in ethanol and examined under a microscope. Chips with weathered surfaces, devitrification spots, or phenocrysts were removed. Crushing, cleaning, and picking was continued at + 40, + 60, + 100, and + 120 mesh until the chips were sufficiently transparent to confirm that they were free of phenocrysts and devitrification spots. Before dissolution, chips were washed for 2 min in 2·5N HCl. Whole-rock powders were processed by sawing slabs from the interiors of fresh samples, polishing off saw marks, and ultrasonicating several times in deionized water. Special care was taken during petrographic examination to ensure that samples

Table 3: Compositional data for volcanic rocks from the northern Mariana Trough dredged during TUNES 7

	57Z	57:1-4*	58:1-3	56:2-5*	55:1-1	54:1-1	53:1-1*	52:1-1	51:1-1
SiO_2	66·74	54·83	52·88	49·09	71·67	50·60	53·85	74·65	54·21
TiO_2	0·90	0·97	1·12	0·84	0·53	0·99	1·10	0·45	1·42
Al_2O_3	14·74	18·30	13·43	18·54	13·29	17·26	16·89	13·85	15·86
FeO*	5·98	9·09	12·69	11·41	3·74	7·69	11·13	2·46	9·49
MgO	1·06	2·01	4·81	4·92	0·49	6·53	3·90	0·38	4·78
CaO	3·97	9·47	8·99	11·39	2·34	11·85	9·28	1·88	9·52
Na_2O	4·88	3·44	2·79	2·26	4·80	2·81	2·72	5·24	3·18
K_2O	1·28	0·98	0·74	0·54	1·52	0·39	0·53	1·56	0·27
P_2O_5	0·24	0·19	0·26	0·17	0·10	0·15	0·13	0·07	0·15
Sum	99·79	99·28	97·71	99·16	98·48	98·27	99·53	100·54	98·88
mg-no.	27	32	45	47	22	64	42	24	52
Q/OL†	Q22	Q6·3	Q5·4	OL1·8	Q31	OL2·2	Q7·0	Q33	Q6·4
K	10440	8300	—	4820	10800	3410	4590	11940	2000
Rb	21·7	17·0	—	11·0	23·2	9·1	9·8	26·2	3·85
Sr	—	496	—	588	243	313	358	212	232
Ba	543	368	—	247	580	99·7	191	501	123
Pb	7·54	3·92	—	2·7	6·94	1·39	2·24	5·71	1·4
La	—	15·5	—	9·75	19·6	8·12	8·65	27·7	4·37
Ce	40·8	29·7	—	19·4	41·9	18·7	17·8	56·2	11·3
Nd	23·5	16·4	—	11·6	23·9	11·4	10·9	29	9·16
Sm	5·87	3·97	—	2·91	5·96	2·91	2·98	6·71	2·86
Eu	—	1·35	—	1·11	1·63	1·1	1·12	2·01	1·11
Gd	—	3·48	—	3·21	6·93	3·48	3·68	7·8	4·02
Dy	—	3·48	—	3·21	7·78	3·46	4·01	8·27	4·22
Er	—	3·00	—	2·18	5·27	2·03	2·58	5·29	2·59
Yb	—	2·90	—	2·16	5·24	1·94	2·49	5·53	2·52
K/Rb	481	488	—	438	466	375	468	456	519
Sr/Nd	—	30·2	—	50·7	10·2	27·5	32·8	7·3	25·4
Ba/La	—	23·7	—	25·3	29·6	12·3	22·1	18·1	28·1
Pb/Ce	0·18	0·13	—	0·14	0·17	0·17	0·13	0·10	0·12
Ba/Pb	72	94	—	91	84	72	85	87	88
$(La/Yb)_N$	—	3·57	—	3·02	2·50	2·80	2·32	3·35	1·16
$^{87}Sr/^{86}Sr$	0·70380	0·70383	0·70423	0·70398	0·70382	0·70346	0·70356	0·70344	0·70365
Leached	—	0·70379	—	0·70391	—	—	0·70358	—	—
$^{143}Nd/^{144}Nd$	0·51297	0·51290	0·51286	0·51290	0·51294	0·51299	0·51293	0·51293	0·51304
ε_{Nd}	+6·7	+5·4	+4·0	+5·3	+6·0	+7·0	+5·9	+5·9	+7·7
$^{206}Pb/^{204}Pb$	18·973	18·921	18·894	18·886	18·924	18·607	18·903	18·755	18·698
$^{207}Pb/^{204}Pb$	15·611	15·585	15·615	15·597	15·560	15·546	15·600	15·564	15·571
$^{208}Pb/^{204}Pb$	38·848	38·728	38·777	38·732	38·670	38·523	38·773	38·599	38·522

	50:1-5*	49:1-1*	66:3-4	68:1-2	48:1-2	48:1-3	48:3-1	47:1-5	46:1-6
SiO_2	50·7	50·91	55·78	52·48	50·29	50·74	51·7	51·22	51·46
TiO_2	0·65	0·90	1·13	1·01	0·82	0·68	0·74	0·96	1·12
Al_2O_3	18·47	18·66	14·50	16·53	17·07	16·93	16·50	16·60	16·95
FeO*	9·02	10·46	9·29	7·51	6·93	7·00	6·74	7·53	7·81
MgO	6·30	3·38	4·13	6·26	7·33	7·47	7·10	7·33	7·07
CaO	12·2	10·94	7·97	11·07	12·82	13·18	12·75	12·12	11·56
Na_2O	1·87	2·31	3·20	2·86	2·45	2·12	1·97	2·49	2·70
K_2O	0·27	0·37	0·31	0·43	0·48	0·49	0·50	0·24	0·22
P_2O_5	0·06	0·11	0·12	0·18	0·16	0·15	0·15	0·13	0·15
Sum	99·54	98·04	96·43	98·33	98·35	98·76	98·15	98·62	99·04
mg-no.	59	40	48	64	69	69	69	67	66
Q/OL	Q2·1	Q4·8	Q11	Q2·5	OL3·6	OL0·2	Q3·1	Q0·8	Q0·8
K	2670	3400	2230	3710	4270	4010	4400	2030	1850
Rb	6·7	6·0	4·22	7·37	8·48	9·29	10·3	3·81	3·01
Sr	346	367	236	310	331	365	406	187	174
Ba	146	224	166	107	137	150	161	58·3	45·8
Pb	1·58	2·59	2·22	2·06	1·38	1·64	4·02	0·838	0·749
La	3·25	4·45	2·8	8·61	9·67	9·86	9·3	4·1	3·79
Ce	7·57	9·9	8·28	19·8	20·0	19·5	18·6	10·7	10·8
Nd	5·31	8·04	7·16	12·0	11·6	10·7	10·2	8·28	8·83
Sm	1·55	2·48	2·39	3·07	2·90	2·35	2·43	2·56	2·82
Eu	0·695	0·969	0·971	1·15	1·05	0·865	0·963	0·980	1·08
Gd	2·30	3·43	3·23	3·54	3·32	2·78	2·52	3·30	3·82
Dy	2·62	3·74	3·97	3·66	3·25	2·54	2·49	3·73	4·33
Er	1·65	2·41	2·51	2·26	1·90	1·50	1·44	2·31	2·70
Yb	1·67	2·43	2·53	2·04	1·80	1·50	1·38	2·23	2·66
K/Rb	399	565	528	503	504	432	427	533	615
Sr/Nd	65·2	45·6	33·0	25·8	28·5	34·1	39·8	22·6	19·7
Ba/La	44·9	50·3	59·3	12·4	14·2	15·2	17·3	14·2	12·1
Pb/Ce	0·21	0·26	0·27	0·10	0·069	0·084	0·22	0·078	0·069
Ba/Pb	92	86	75	52	99	91	40	70	61
$(La/Yb)_N$	1·30	1·22	0·74	2·82	3·59	4·40	4·51	1·23	0·95
$^{87}Sr/^{86}Sr$	0·70353	0·70410	0·70336	0·70299	0·70335	0·70323	0·70339	0·70303	0·70293
Leached	0·70354	0·70396	—	—	—	—	—	—	—
$^{143}Nd/^{144}Nd$	0·51297	0·51298	0·51303	0·51301	0·51296	0·51293	—	0·51302	0·51309
ε_{Nd}	+6·7	+6·9	+7·9	+7·4	+6·2	+5·9	—	+8·1	+9·1
$^{206}Pb/^{204}Pb$	18·944	18·850	18·854	18·501	18·708	18·785	18·671	18·720	18·488
$^{207}Pb/^{204}Pb$	15·586	15·557	15·579	15·523	15·571	15·543	15·551	15·570	15·478
$^{208}Pb/^{204}Pb$	38·735	38·659	38·684	38·194	38·435	38·432	38·359	38·465	38·081

Table 3: continued

	46:1-8	71:1-14	45:5-2*	72:2	73:1-1	73:2-1	74:1-1	76:1-1	75:1-2
SiO_2	52·37	51·70	51·32	51·57	50·98	51·9	51·09	52·79	52·30
TiO_2	1·17	1·11	1·22	1·27	1·36	1·41	1·13	1·62	1·61
Al_2O_3	16·66	16·50	17·10	16·92	17·00	17·15	17·83	15·88	16·38
FeO*	7·55	7·72	8·40	7·34	7·75	7·82	7·22	9·48	8·38
MgO	7·25	6·34	6·74	6·55	7·28	6·69	7·72	7·23	7·33
CaO	11·29	11·70	11·36	10·57	10·40	10·53	11·83	10·37	10·60
Na_2O	2·45	2·99	2·89	3·09	3·46	3·56	2·75	3·48	3·27
K_2O	0·21	0·42	0·40	0·48	0·35	0·33	0·30	0·23	0·35
P_2O_5	0·15	0·20	0·15	0·18	0·17	0·18	0·17	0·18	0·18
Sum	99·1	98·68	99·58	97·97	98·75	99·57	100·04	101·26	100·40
mg-no.	67	64	63	65	67	64	69	62	65
Q/OL	Q3·3	Q0·4	Q2·7	Q0·5	OL6·8	OL3·8	OL3·8	OL1·7	OL1·3
K	1790	3560	3540	4440	3140	3070	2570	2040	3150
Rb	3·17	7·09	5·95	8·34	4·71	4·14	4·3	2·34	4·12
Sr	183	306	204	262	268	239	265	184	200
Ba	45·8	94·4	50·7	87·9	49·6	45·0	40·6	27·3	42·3
Pb	0·71	1·16	1·10	1·19	0·91	0·89	0·70	0·75	0·78
La	4·43	9·02	4·34	7·75	6·19	5·89	6·05	5·31	7·72
Ce	11·7	20·3	13·3	19·1	15·6	16·1	14·5	15·1	17·8
Nd	9·55	12·7	10·1	12·6	11·0	11·6	10·3	12·4	12·7
Sm	3·06	3·33	3·08	3·54	3·24	3·42	3·00	3·97	3·77
Eu	1·17	1·19	1·13	1·28	1·25	1·32	1·13	1·48	1·36
Gd	4·22	4·03	4·16	4·40	4·15	4·40	4·03	5·27	4·84
Dy	4·72	4·02	4·56	4·73	4·66	4·83	4·24	5·98	5·36
Er	3·03	2·45	2·82	2·92	2·85	3·05	2·62	3·74	3·29
Yb	2·95	2·58	2·72	2·84	2·74	2·90	2·50	3·63	3·20
K/Rb	565	502	595	532	667	742	598	872	765
Sr/Nd	19·2	24·1	20·2	20·8	24·4	20·6	25·7	14·8	15·7
Ba/La	10·3	10·5	11·7	11·3	8·0	7·6	6·7	5·1	5·5
Pb/Ce	0·061	0·057	0·083	0·062	0·058	0·055	0·048	0·050	0·044
Ba/Pb	65	81	46	74	55	51	58	36	54
$(La/Yb)_N$	1·00	2·34	1·07	1·82	1·51	1·36	1·62	0·98	1·61
$^{87}Sr/^{86}Sr$	0·70293	0·70301	—	0·70307	0·70301	0·70287	0·70288	0·70279	0·70277
Leached	—	—	0·70307	—	—	—	—	—	—
$^{143}Nd/^{144}Nd$	0·51307	0·51300	—	0·51306	0·51312	0·51310	0·51308	0·51313	0·51309
εNd	+8·7	+7·2	—	+8·4	+9·5	+9·3	+8·9	+9·8	+9·1
$^{206}Pb/^{204}Pb$	18·564	18·583	18·487	18·496	18·247	18·155	18·310	17·970	17·965
$^{207}Pb/^{204}Pb$	15·556	15·557	15·498	15·514	15·490	15·469	15·487	15·437	15·426
$^{208}Pb/^{204}Pb$	38·340	38·286	38·117	38·142	37·925	37·827	37·955	37·659	37·645

	79:1-1	80:1-3	82:1-1	SMT	MORB	ARC
SiO_2	50·46	49·56	51·40	51·0	50·45	50·52
TiO_2	1·05	0·84	1·27	1·27	1·62	1·04
Al_2O_3	17·10	17·93	16·60	16·5	15·26	16·94
FeO*	7·84	8·61	7·94	8·4	10·43	11·02
MgO	7·58	8·60	6·43	6·8	7·58	5·37
CaO	11·48	11·55	11·22	11·3	11·30	10·75
Na_2O	3·13	2·40	3·07	3·0	2·68	2·68
K_2O	0·17	0·35	0·24	0·29	0·10	0·76
P_2O_5	0·13	0·14	0·17	0·15	—	0·18
Sum	98·94	99·98	98·34	98·71	99·42	99·26
mg-no.	67	67	63	63		
Q/OL	OL7·8	OL9·8	Q0·5			
K	1530	3200	2230	2340	884	5370
Rb	2·63	12·3	4·26	3·7	1·26	7·42
Sr	224	188	214	201	113	329
Ba	30·9	28·3	40·6	44·6	13·9	141
Pb	0·61	0·49	0·78	0·70	0·49	4·05
La	4·32	3·49	5·30	4·54	3·90	6·41
Ce	11·9	8·62	14·7	12·0	12·0	13·90
Nd	9·55	7·03	11·7	10·5	11·2	9·80
Sm	3·00	2·38	3·61	3·0	3·75	2·69
Eu	1·20	0·994	1·36	1·6	1·34	0·93
Gd	3·93	3·33	4·60	4·0	5·08	3·14
Dy	4·47	4·28	5·22	4·5	6·30	3·29
Er	2·80	2·85	3·23	2·8	4·14	2·03
Yb	2·69	2·83	3·06	2·7	3·90	1·95
K/Rb	582	260	523	630	702	724
Sr/Nd	23·5	26·7	18·3	19	10·1	33·6
Ba/La	7·2	8·1	7·7	9·8	3·6	22·0
Pb/Ce	0·051	0·057	0·053	0·058	0·041	0·29
Ba/Pb	51	58	52	64	28	—
$(La/Yb)_N$	1·07	0·82	1·73	1·1	0·67	2·2
$^{87}Sr/^{86}Sr$	0·70279	0·70314	0·70281	0·70285	0·70286	0·70337
$^{143}Nd/^{144}Nd$	0·51311	0·51299	0·51308	0·51310	0·51313	0·51297
ε_{Nd}	+8·9	+7·0	+8·8	+9·3	+9·5	+6·5
$^{206}Pb/^{204}Pb$	18·221	18·446	18·254	18·213	18·575	18·686
$^{207}Pb/^{204}Pb$	15·456	15·539	15·487	15·479	15·486	15·556
$^{208}Pb/^{204}Pb$	37·832	38·207	37·945	37·896	37·968	18·310

*Whole-rock powder. All other analyses use glass separates.
†Normative % quartz (Q) or olivine (OL).
SMT, average of 22 BABB from the southern Mariana Trough (Gribble *et al.*, 1996). MORB, average of 26 fresh MORB glasses (Hofmann, 1988); isotopic compositions are averaged Indian, Pacific, and Atlantic MORB data from Zindler *et al.* (1982). ARC, typical Mariana Arc basalt (AG4); data from Schmidt (1957) and White & Patchett (1984); Pb data represent average Agrigan data from Woodhead & Fraser (1985). Pb content inferred from Pb/Ce for Kasuga 1 (Stern *et al.*, 1993).

were selected with no visible signs of alteration; this was monitored by analyzing $^{87}Sr/^{86}Sr$ before and after leaching whole-rock powders in 6N HCl.

Approximately 70–100 mg of glass or powder was dissolved and analyzed for Nd and Sr isotopic compositions and LILE and REE concentrations. Standard

isotope dilution and cation exchange techniques were used to separate LILE (K, Rb, Sr, and Ba) and REE (La, Ce, Nd, Sm, Eu, Gd, Dy, Er, and Yb). A procedure modified after Richard *et al.* (1976) was used to further isolate Ba, La, and Ce for isotope dilution analysis and separate Nd from Sm for isotope composition runs. Pb analyses required 15–30 mg of sample for isotope dilution and sufficient sample (70–270 mg) for a 90–100 ng processing load for isotope composition runs. The Pb separation procedure has been reported by Manton (1988), with an initial anion column separation. Total processing blanks were: Pb, <140 pg; Nd, < 700 pg; Sr, < 2 ng. Sr and Nd isotopic compositions were determined with a Finnigan MAT 261 multi-collector TIMS in dynamic mode. Sr isotopic compositions were fractionation-corrected to $^{86}Sr/^{88}Sr = 0{\cdot}1194$ and adjusted relative to E&A $SrCO_3$ $^{87}Sr/^{86}Sr = 0{\cdot}70800$. Nd isotopic compositions were fractionation-corrected to $^{146}Nd/^{144}Nd = 0{\cdot}7219$ and ε_{Nd} was calculated using the ε_{Nd} values of Pier *et al.* (1989) for BCR-1 and UCSD standards. The Pb fractionation correction was 0·15%/a.m.u. Standard averages and reproducibility of standards (±2 SD) over the period of data collection were as follows: E&A $SrCO_3$ $^{87}Sr/^{86}Sr = 0{\cdot}708018(0{\cdot}000049)$, UCSD $^{143}Nd/^{144}Nd = 0{\cdot}511848(0{\cdot}000029)$, BCR-1 $^{143}Nd/^{144}Nd = 0{\cdot}512647$ and NBS 981 after fractionation correction: $^{206}Pb/^{204}Pb = 16{\cdot}948(0{\cdot}020)$, $^{207}Pb/^{204}Pb = 15{\cdot}502(0{\cdot}025)$, and $^{208}Pb/^{204}Pb = 36{\cdot}755(0{\cdot}083)$.

RESULTS

Northern Mariana Trough glasses and whole-rock analyses (Table 3) display a northward shift to a wider range and higher average silica content (Fig. 3). South of the VTZ, lavas are predominantly low-K basalt or, less commonly, basaltic andesite—except for the D73 suite, which straddles the low-K–medium-K boundary. The southern VTZ suite [including data for MTB-22 reported by Stern *et al.* (1990)] is partitioned into low- and medium-K basalt but includes low-K basaltic andesite. The northern VTZ suite is distinct in K_2O–SiO_2 space and includes medium-K dacite and rhyolite.

Plots of moderately incompatible elements Na_2O and TiO_2 vs MgO show that NMT glasses range in composition between Spread BABB and Mariana Arc lavas (Fig. 4). The field defined by Spreading Ridge samples completely overlaps the SMT and MTB-18 field, showing that the composition of Mariana Trough Spread BABB is petrologically coherent. Central Graben samples are indistinguishable from Spread BABB, and are included with these for the purposes of defining the field 'Central Graben & Spreading Ridge'. The SVTZ glasses form an extension of the Mariana Arc glass tephra trend (Lee *et al.*, 1995) but fall in the field of Spread BABB. In contrast, NVTZ lavas are indistinguishable from Mariana Arc lavas.

Lavas with *mg*-number >65 were recast into mineral compositions on the basis of molar oxygen proportions (Tormey *et al.*, 1987) and plotted in phase diagrams on projections from plagioclase and olivine. Spreading Ridge and Central Graben lavas form a relatively tight group enclosed by the SMT and MTB-18 field in both projections; MTB-22 samples plot in a similar field. Other SVTZ samples display a much larger range in normative mineralogy. Individual suites are parallel (from olivine) or nearly parallel (from plagioclase) to the 1 atm cotectic. Most dredge suites have a narrow range in *mg*-number so that it is unlikely that these suites are related by crystal fractionation of a common parent. Kinzler & Grove (1992) developed a petrogenetic grid for accumulated melt fractions in a polybaric melt regime. NMT suites align parallel to the variable melt percent, constant pressure vector, and for samples with calculated *F* (degree of mantle melting) show the proper relative order in percent melt. This indicates that these trends reflect variable degrees of melting at a common temperature–pressure interval along a lherzolite assemblage + melt cotectic. Lavas become increasingly oversaturated in silica northward along the extension axis. Quartz-normative compositions predominate in the NVTZ, SVTZ, and Central Graben, whereas olivine-normative compositions dominate the Spreading Ridge suite.

Trace element abundances vary systematically along the extension axis, with patterns of normalized trace elements becoming flatter and smoother moving from the NVTZ (Fig. 5a) through the SVTZ (Fig. 5b) and Central Graben (Fig. 5c) to the Spreading Ridge (Fig. 5d). This systematic behavior reflects two effects, both of which become increasingly important towards the north: (1) increased fractionation of fluid mobile elements (LILE, Sr, Pb) relative to REE; (2) fractionation of LREE relative to HREE. The first effect indicates that a fluid-mobile 'subduction component' becomes more important to the north, and we will show later that the second effect indicates that the degree of melting increases in the same direction. Mariana Trough Spread BABB show variable enrichment in a subduction component which is revealed both isotopically and in terms of trace element abundances, as is shown in Fig. 5d by noticeable spikes in Pb and Sr and an overall enrichment in K, Rb, and Ba. There is no obvious difference in trace element abundances between Spreading Ridge and SMT samples, although Spreading Ridge samples do not include the very MORB-like basalts recovered from near 15°N (Gribble *et al.*, 1996).

HREE abundances are higher in the Central Graben and Spreading Ridge lavas than in VTZ basalts, whereas LREE concentrations increase irregularly to the north (Fig. 6). La_N/Yb_N ratios in the Spreading Ridge basalts

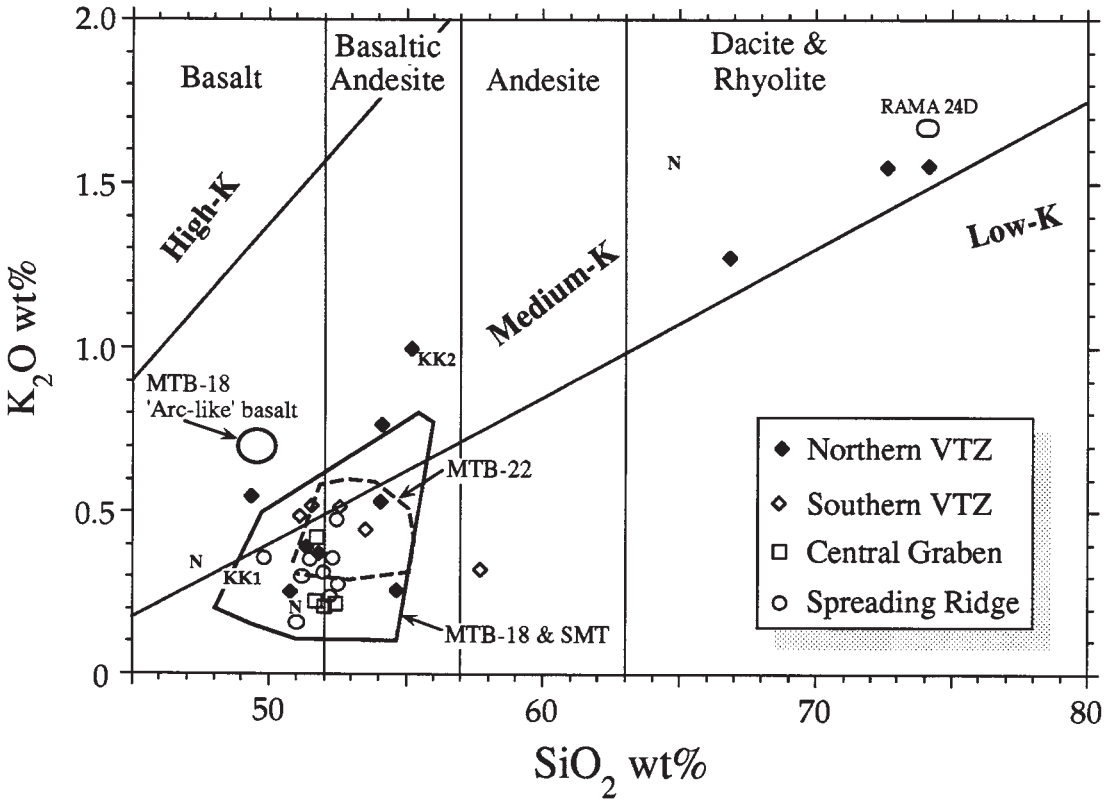

Fig. 3. K_2O vs SiO_2 diagram for samples from the northern Mariana Trough analyzed for this study. Dredge glasses are predominantly basaltic, except for N-VTZ samples, which extend to medium-K rhyolite. The samples from Nikko (where the back-arc extension axis intersects the arc) are plagioclase-bearing whole rocks (Bloomer *et al.*, 1989*a*) and are labeled 'N'. The MTB-18 'Arc-like' basalt field is from ALVIN dive A1846 (Hawkins *et al.*, 1990). Also shown are fields defined by samples from previous studies in the NMT, including dredges KK1 and KK2 from the Northern VTZ during a cruise by the *Kana Keoki* in 1984 (Jackson, 1989) and MTB-22 basalts from the Southern VTZ (Stern *et al.*, 1990). RAMA 24D corresponds to the composition of felsic lavas studied by Lonsdale & Hawkins (1985) from the off-axis 'mounds' hydrothermal field at 18°N. All samples are renormalized to 100% anhydrous. The silica and K_2O boundaries are from LeMaitre (1989).

range from slightly less to slightly greater than one. Basalts from the Central Graben have patterns that are subparallel to but lower than Spreading Ridge lavas. Among the Central Graben basalts, D71:1-14 is anomalous in having an REE pattern that is similar to southern VTZ samples. Most SVTZ basalts [MTB-22 data of Stern *et al.* (1990) and D68 and D48] are LREE enriched (La_N/Yb_N = 1·4–4·5). The D48 suite has the lowest HREE abundances (Yb = 6 × to 9 × chondrite) reported for Mariana Trough lavas and, excluding evolved NVTZ samples, the highest LREE abundances. The D48 suite has the highest La_N/Yb_N (3·6–4·5) for any Mariana Trough sample. NVTZ lavas have REE abundances that span the range reported for the rest of the Mariana Trough but can be subdivided into two groups. Basalts from the southern part of the NVTZ have flat REE patterns (La_N/Yb_N = 1·16–1·3), whereas those from the northern NVTZ are enriched in the LREE (La_N/Yb_N = 2·8–3). NVTZ basaltic andesites are from the northern part of the NVTZ and are similar to the basalts from this region in their LREE enrichment (La_N/Yb_N = 2·3–3·6).

The similarity between Rift BABB and arc lavas can also be seen in plots of incompatible element ratios that distinguish between Spread BABB and Mariana Arc lavas (Fig. 7). Ratios of incompatible elements such as Ce to Pb, K to Rb, La to Yb, and Ba to La should not change significantly as a result of moderate degrees of low-pressure fractionation, and can be expected to reflect the ratios developed when melt generation occurred. Lavas from intra-oceanic arcs are characterized by high Ba/La and low Ce/Pb coupled with low $(La/Yb)_N$ and moderate K/Rb. Mariana Arc lavas show a strong inverse correlation between Ba/La and $(La/Yb)_N$, interpreted by Lin *et al.* (1989) to indicate mixing. Mariana Arc lavas are further characterized by moderate K/Rb (300–600) and low Ce/Pb (<10). In contrast, Mariana Trough Spread BABB have low Ba/La (<20), low $(La/Yb)_N$ (<2), moderate to high K/Rb (up to >1200), and high Ce/Pb (>10). The fields defined by Mariana Trough Spread

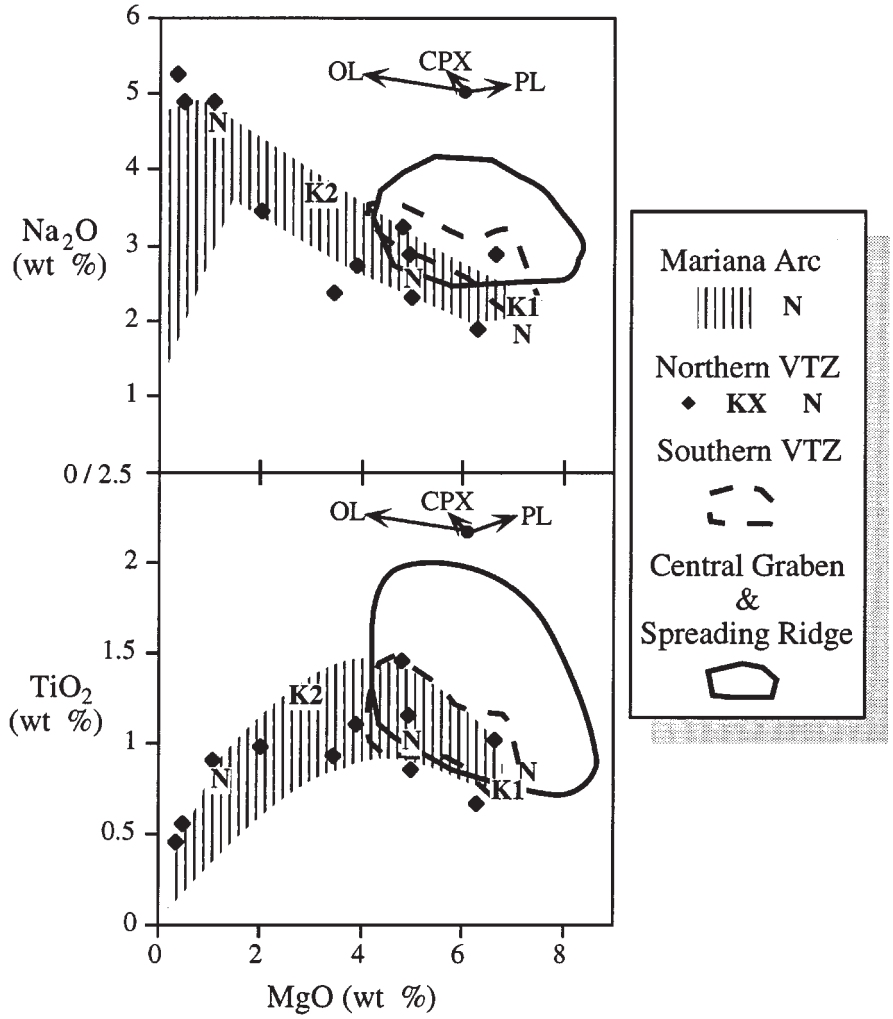

Fig. 4. Plot of the moderately incompatible elements Na_2O and TiO_2 vs MgO. Central Graben samples are grouped with samples from the well-defined spreading ridge segments to the south, including Spreading Ridge, MTB-18, and SMT. Mariana Arc fields are defined by tephra glasses studied by Lee *et al.* (1995). The SVTZ fields include MTB-22 data (Stern *et al.*, 1990) and the NVTZ fields include two *Kana Keoki* dredges (K1 and K2; Jackson, 1989). Data for Nikko are shown with 'N' and are listed as belonging to both the NVTZ and Mariana Arc. MTB-18 data include samples reported by Fryer *et al.* (1981), Hawkins & Melchior (1985), Sinton & Fryer (1987), Volpe *et al.* (1987), and Hawkins *et al.* (1990). SMT data are from Gribble *et al.* (1996). The labeled arrows show magmatic evolution accompanying 5% fractionation of phenocryst core compositions from relatively primitive glasses analyzed by Hawkins & Melchior (1985). The similarity of NVTZ samples to Mariana Arc and similarity of SVTZ samples to those recovered from the spreading ridges to the south should be noted.

BABB on plots of Ba/La vs $(La/Yb)_N$ and K/Rb vs Ce/Pb (Fig. 7) encompass the 'mean N-MORB' of Hofmann (1988). In spite of the fact that much of the variability in the field of Spread BABB results from addition of a subduction component to an N-MORB mantle source (Stolper & Newman, 1994; Gribble *et al.*, 1996), there is no overlap between arc and Spread BABB fields (Fig. 7). Data for NMT Rift BABB span arc and Spread BABB fields; at one end, Spreading Ridge and Central Graben basalts are very similar to Spread BABB, whereas NVTZ samples can scarcely be distinguished from Mariana Arc basalts. SVTZ samples [including MTB-22 data of Stern *et al.* (1990)] span fields defined by arc plus NVTZ samples on the one hand and Spreading Ridge plus Central Graben plus Spread BABB samples on the other.

Lavas from the Mariana Arc and Spread BABB from the Mariana Trough can be distinguished by their Sr, Nd, and Pb isotopic compositions. NMT data overlap and bridge these two fields (Figs 8 and 9). For all three isotopic systems, Spreading Ridge samples are indistinguishable from Spread BABB, whereas the isotopic compositions of Rift BABB northward become

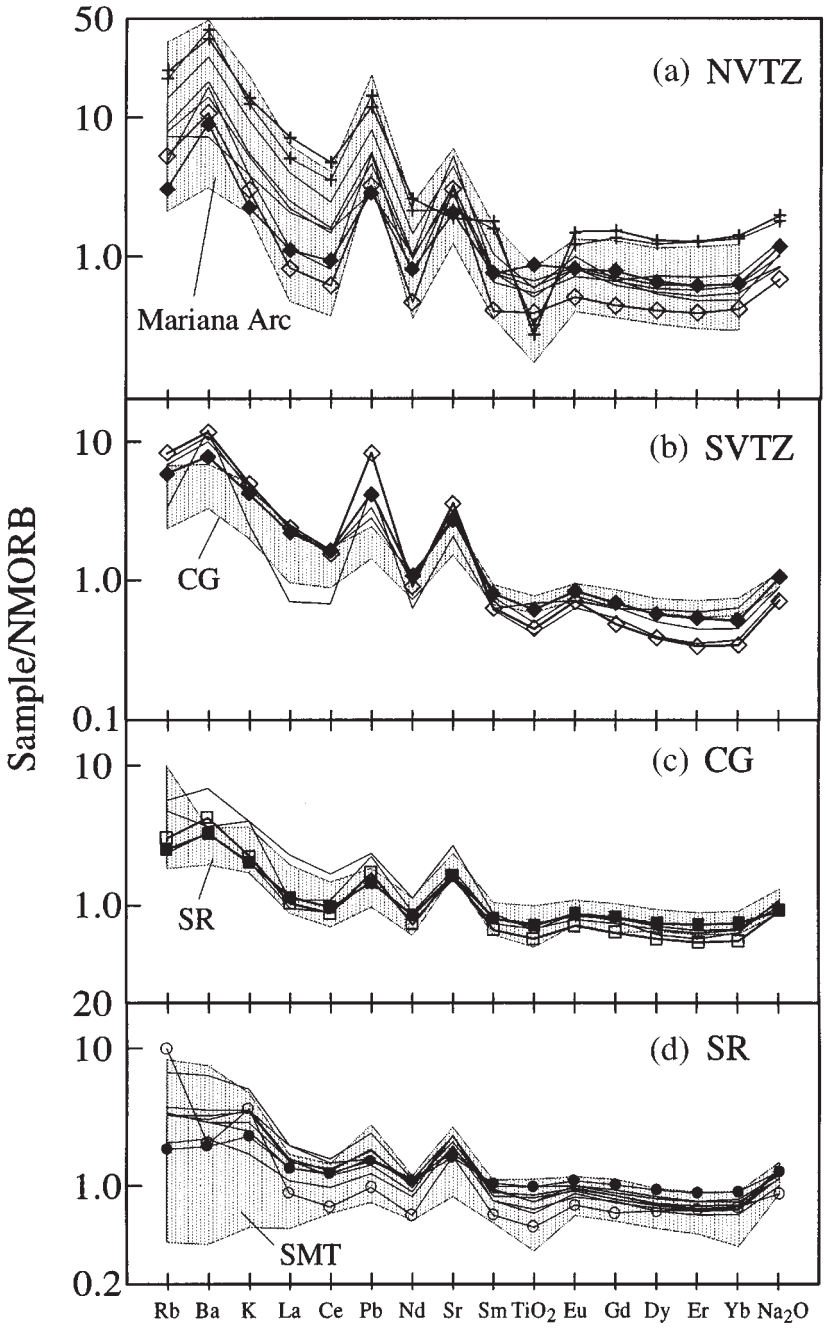

Fig. 5. Compatibility diagram, with order of elements and N-MORB normalizing values after Hofmann (1988). (a) Individual trace element patterns for NVTZ lavas are compared with Mariana Arc lavas (stippled field). (Note the similar trace element patterns for NVTZ and Mariana Arc lavas, including 'spikes' in Ba, Pb, and Sr; patterns with '+' are NVTZ felsic samples 55:1-1 and 52:1-1.) (b) SVTZ trace element patterns; MTB-22 data reported by Stern *et al.* (1990; not shown) show similar patterns to the four SVTZ samples plotted. Stippled field outlines data for basalts from the Central Graben. (c) Trace element patterns for Central Graben basalts, compared with a stippled field outlining data from the spreading ridge between 19°50′ and 18°45′N (SR). (d) Trace element patterns for Spreading Ridge basalts compared with SMT data (Gribble *et al.*, 1996). For the sake of clarity, MTB-22 data (Stern *et al.*, 1990) are not shown with the SVTZ samples but display similar patterns. Open and closed symbols are shown for samples with the highest and lowest degrees of melting, respectively, within each defined segment for NMT basalts, as calculated by the model presented in the discussion. (Note that for the N- and S-VTZ data the high-degree-melt lavas have lower TiO_2 and HREE, but higher LILE and Pb concentrations than the low-degree-melt lavas.)

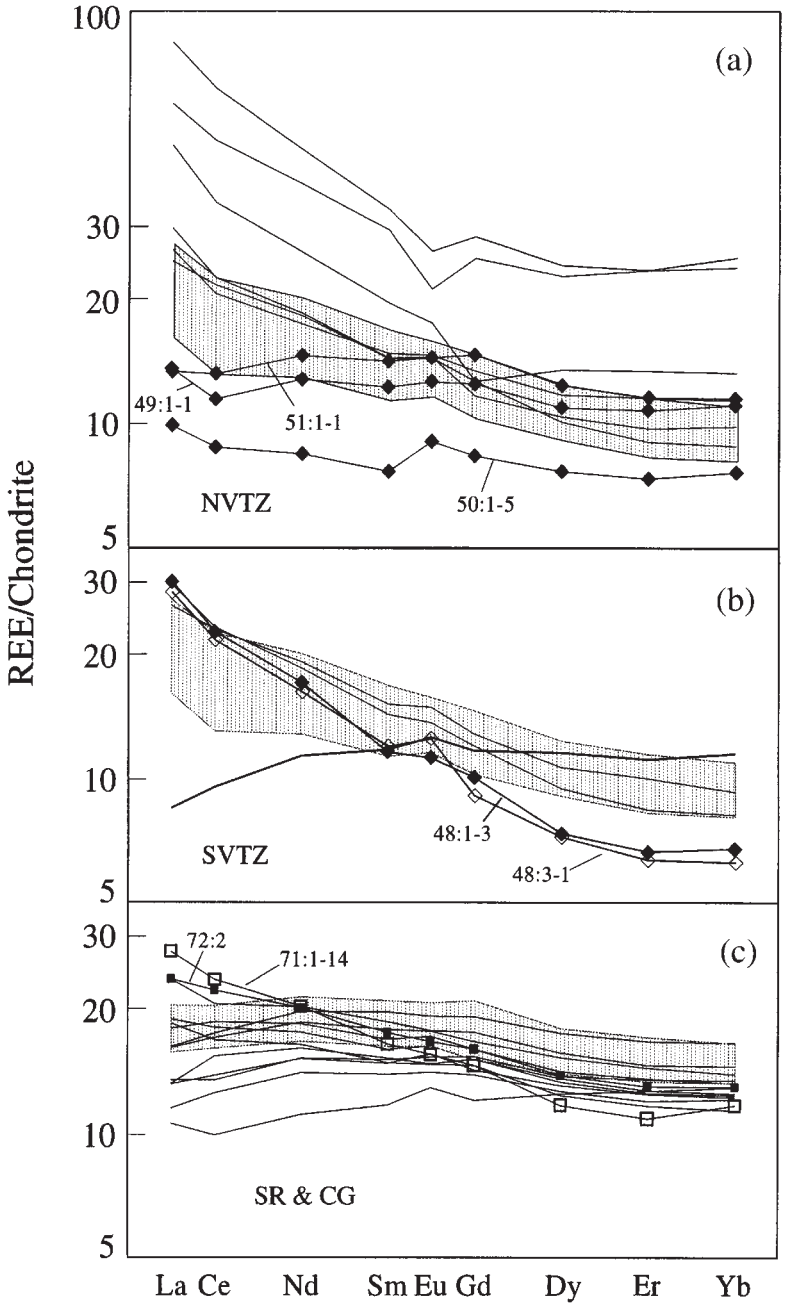

Fig. 6. Chondrite-normalized REE plots for (a) Northern VTZ, (b) Southern VTZ, and (c) Central Graben and Spreading Ridge between 19°50′ and 18°45′N. Shaded field in (a) and (b) outlines REE data for MTB-22 (Stern *et al.*, 1990). Shaded field in (c) outlines REE data for basalts from the southern Mariana Trough (Gribble *et al.*, 1996). Samples discussed in the text are identified. Symbols are as in Fig. 3 except for 72:2 in (c) which is from the spreading Ridge portion of the MT.

more like those of the Mariana Arc (Fig. 10). A particularly strong Pb isotopic gradient is observed. NVTZ samples cannot be distinguished from Mariana Arc lavas, and SVTZ lavas are intermediate between these two fields. Central Graben basalts overlap Spread BABB but towards the arc fields. $^{206}Pb/^{204}Pb$ >18·5 is found for both arc and BABB basalts, but $^{206}Pb/^{204}Pb$ <18·5 is restricted to Spread BABB. $^{206}Pb/^{204}Pb$ for VTZ and

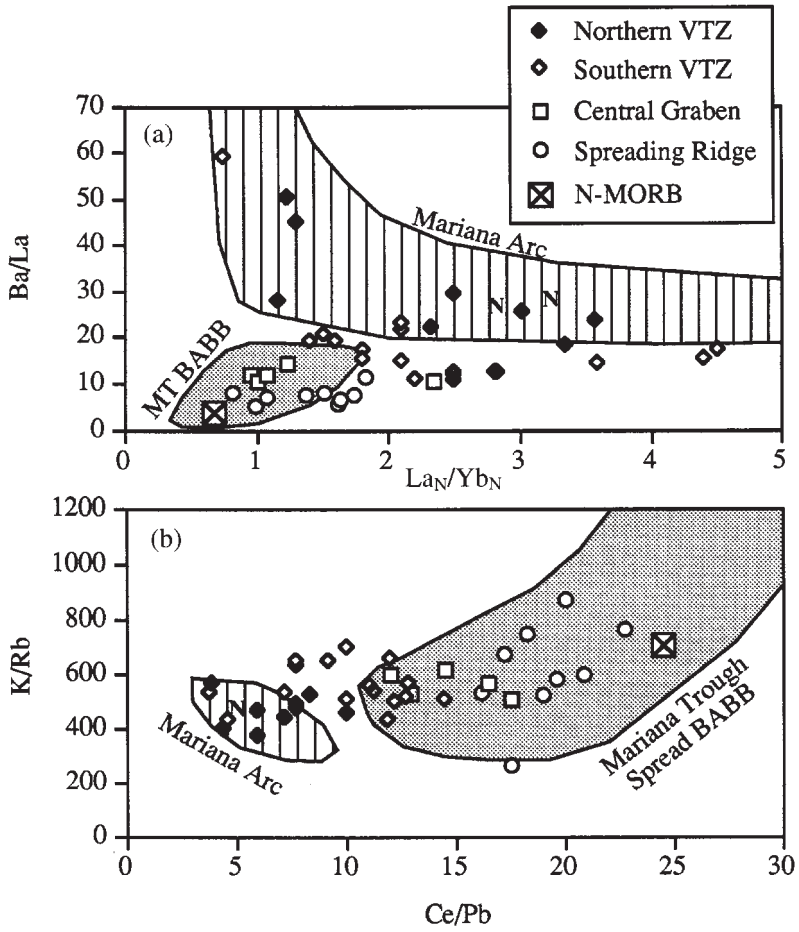

Fig. 7. Diagnostic trace element ratios for NMT samples compared with fields for the active Mariana Arc and BABB from Mariana Trough spreading ridges. (a) Ba/La vs La_N/Yb_N, modified after Lin *et al.* (1989); (b) K/Rb vs Ce/Pb. It should be noted that Mariana Arc and Spread BABB (SMT or MTB-18 + SMT) are completely resolved on both plots, and that Spreading Ridge and Central Graben samples plot in the field for Spread BABB (or nearly so), whereas NVTZ samples plot in the field for the Mariana Arc. SVTZ data plot between fields defined by Mariana Arc and NVTZ on the one hand and Spread BABB + Spreading Ridge + Central Graben on the other hand.

Central Graben samples are invariably >18·48 (although felsic CG samples have $^{206}Pb/^{204}Pb$ = 18·2–18·3, Stern *et al.*, 1996). Spreading Ridge samples include $^{206}Pb/^{204}Pb$ <18·45; sample 73:1-1 at 18°44′N has $^{206}Pb/^{204}Pb$ = 18·25, and $^{206}Pb/^{204}Pb$ <18·0 is found for D76 and D75 at 19°27′N. VTZ samples form an array that extends from Spread BABB to the high $^{206}Pb/^{204}Pb$ Mariana Arc compositions. Therefore, VTZ lavas lie partly outside the Mariana Arc field at relatively high $^{207}Pb/^{204}Pb$ and $^{208}Pb/^{204}Pb$.

Sr and Nd isotopic compositions show the similarity of NVTZ samples to the Mariana Arc, the similarity of Spreading Ridge plus Central Graben to Spread BABB, and the transitional nature of SVTZ samples (Fig. 9). NVTZ samples also show the displacement towards higher $^{87}Sr/^{86}Sr$ at a given ε_{Nd} that is characteristic of all arc lavas (Fig. 9a; Stern *et al.*, 1993). Two NVTZ samples have higher $^{87}Sr/^{86}Sr$ than the highest value reported for the Mariana Arc (D58:1-3 and D49:1-1). A plot of $^{87}Sr/^{86}Sr$ vs $^{206}Pb/^{204}Pb$ (Fig. 9b) serves to emphasize two important aspects of the data: (1) the similarity of NVTZ lavas to those of the Mariana Arc; and (2) the similarity of basalts from the Spreading Ridge plus Central Graben to the larger group of Mariana Trough Spread BABB.

Water and carbon dioxide concentrations are listed in Table 4. Most of the glasses are supersaturated with respect to the mixed volatile system at the pressure corresponding to the depth of collection. Because CO_2 is so much less soluble than water in silicate melts, any glasses that contain significant CO_2 (>~50 ppm) generally cannot have degassed H_2O as a result of decompression, because virtually all CO_2 is lost before any significant

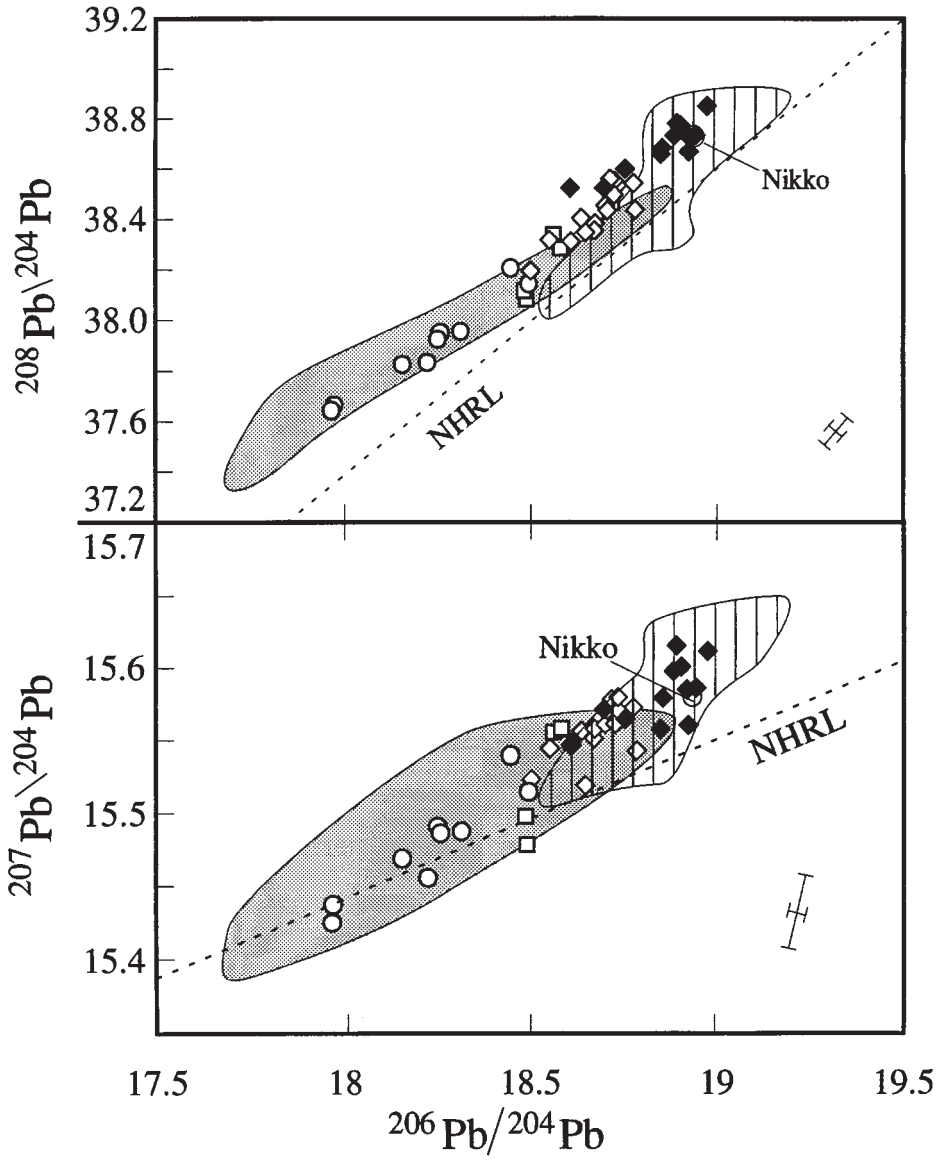

Fig. 8. Pb isotopic data. The NHRL is the Northern Hemisphere Regression Line of Hart (1984). The field for spreading ridge segments, SMT + MTB-18, is from Volpe *et al.* (1990) and Gribble *et al.* (1996). Mariana Arc data are from sources listed by Stern *et al.* (1993) and J. Morris *et al.* (unpublished data, 1997). Symbols are as in Fig. 3.

water exsolves. For example, Dixon *et al.* (1995) showed that the pure volatile phase in basaltic magmas at 400 bar (4000 m water depth) is saturated with H_2O = 2·00 wt % and CO_2 = 185 ppm. Among the NMT samples, only 48:1-3 contains no CO_2, and the water content of this sample is close to saturation, given the errors involved. Therefore, and with the exception of 48:1-3, the water data are interpreted as approximating magmatic water concentrations.

There may be a latitudinal variation of water content in these glasses. With the exception of 72:2 at the northern tip of the propagating ridge, Spreading Ridge samples generally contain less water (0·5– 1·6% H_2O) relative to VTZ samples (1·4–1·9% H_2O). The range observed for Spreading Ridge samples is less than that found for the SMT (0·2–2·8%; Gribble *et al.*, 1996) and MTB-18 (0·49–2·1% H_2O; Stolper & Newman, 1994). Both Spread and Rift BABB from the Mariana Trough are

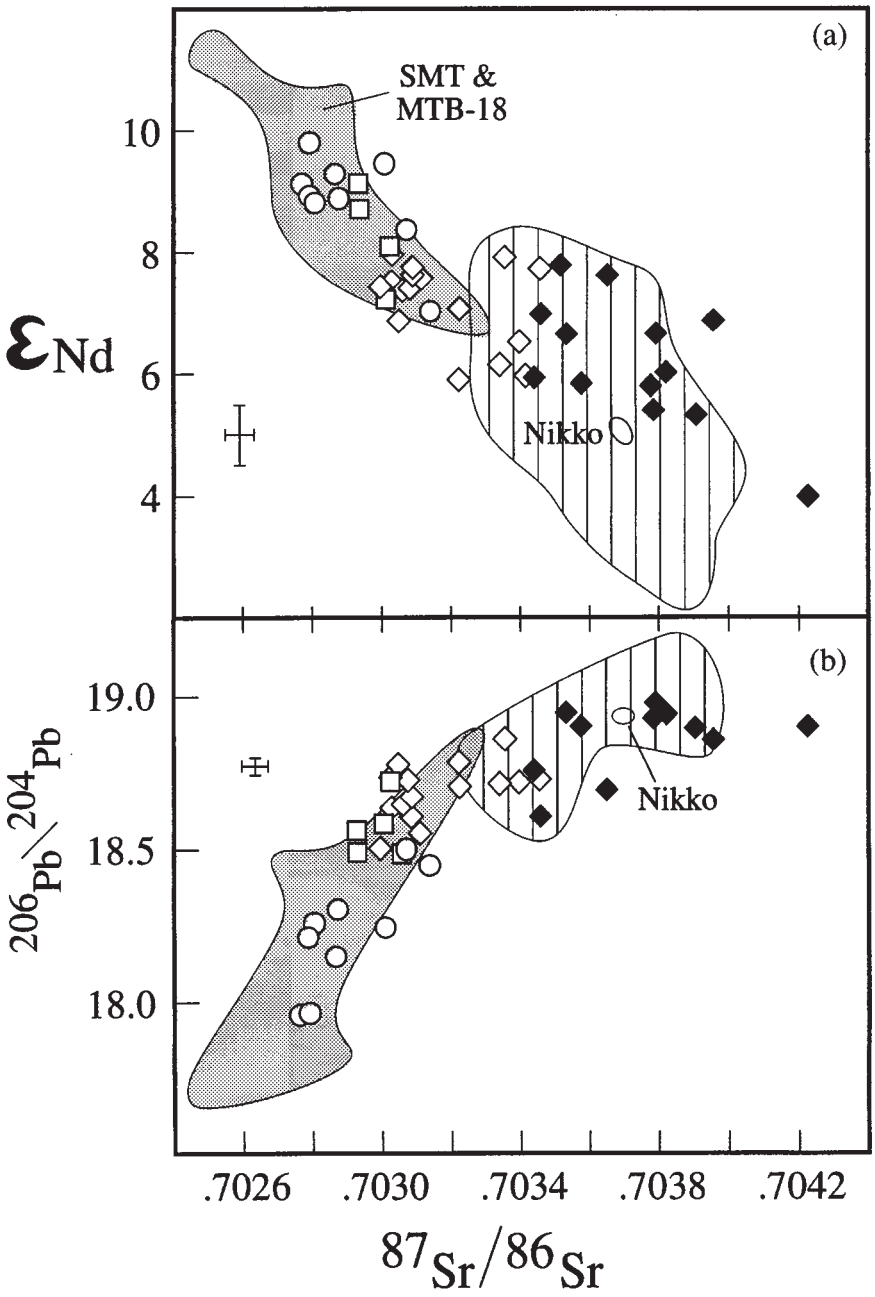

Fig. 9. Sr–Nd–Pb isotopic systematics for NMT samples compared with fields occupied by Spread BABB (MTB-18 + SMT) and the active Mariana Arc. Symbols are as in Fig. 3. (a) ε_{Nd} vs $^{87}Sr/^{86}Sr$. (b) $^{87}Sr/^{86}Sr$ vs $^{206}Pb/^{204}Pb$. It should be noted that Spreading Ridge samples are indistinguishable from Spread BABB and that NVTZ samples are indistinguishable from Mariana Arc lavas, whereas SVTZ lavas bridge these two fields. Central Graben basalts lie in the fields of Spread BABB but towards the arc fields.

generally wetter than Lau Basin BABB, which contains 0·22–1·6% H_2O (Danyushevsky *et al.*, 1993). As is generally true for BABB, Mariana Trough BABB are much wetter than MORB (0·1–0·4% H_2O; Dixon *et al.*, 1988). With the exception of felsic sample 55:1-1, all Mariana Trough samples cluster around $K_2O/H_2O = 0·25$, which is characteristic of BABB (Danyushevsky *et al.*, 1993).

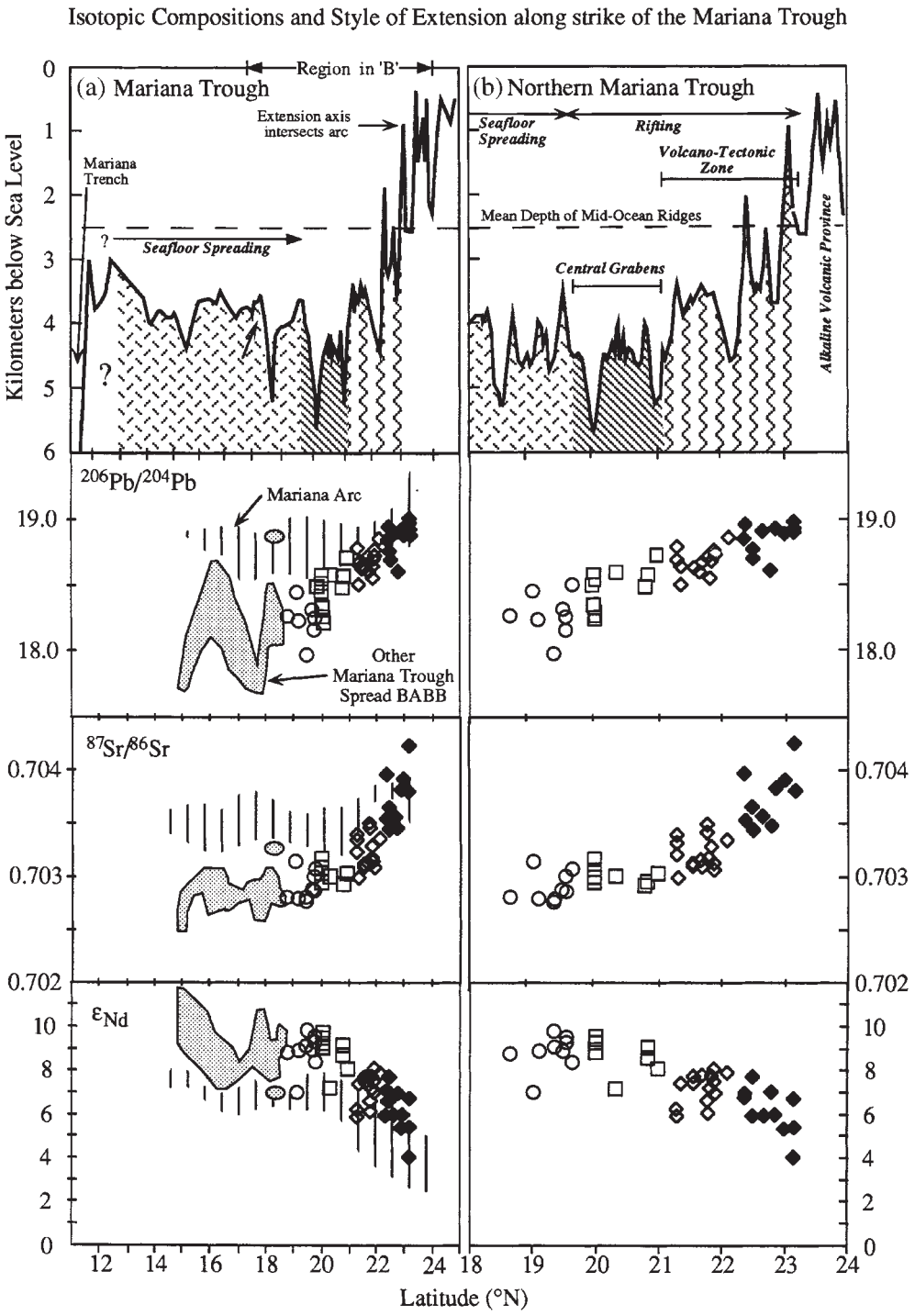

Fig. 10. Latitude and style of extension vs $^{206}Pb/^{204}Pb$, $^{87}Sr/^{86}Sr$, and ε_{Nd}. It should be noted that the intermediate-scale variations observed in the southern Mariana Trough are replaced north of 18° by a monotonous increase in $^{206}Pb/^{204}Pb$, $^{87}Sr/^{86}Sr$, and ε_{Nd}. The distinction between arc and back-arc basin sources that is so clear in that part of the system where spreading is occurring is progressively obscured to the north where rifting is occurring.

Table 4: H_2O and CO_2 contents in glasses from the northern Mariana Trough (arranged from north to south)

Sample	% H_2O	*N**	SD	ppm CO_2	*N**	SD
55:1-1	1·51	4	0·13	290	4	20
54:1-1	1·693	4	0·017	98	4	37
68:1-2	1·87	4	0·09	100	4	24
48:1-3	1·57	4	0·09	3	4	20
47:1-5	1·76	4	0·08	82	4	8
46:1-6	1·41	4	0·09	137	4	11
71:1-14	1·82	3	0·36	158	4	20
72:2	2·23	4	0·09	81	4	25
73:2-1	1·153	4	0·047	196	4	23
74:1-1	1·00	4	0·07	137	4	5
76:1-1	0·729	3	0·006	221	3	20
80:1-3	0·571	4	0·003	362	4	8
82:1-1	1·69	3	0·20	134	4	22

*Number of determinations.

DISCUSSION

In the following discussion, we consider three related problems of global significance from the perspective of our data set for the Mariana Trough. First, we comment briefly on the controversy of whether or not arc and back-arc basin igneous activity is synchronous in a single back-arc basin system. Second, we address questions related to the degree of melting along strike of the extension axis, and the different petrogenetic styles along the strike of the extension axis. Finally, we discuss the composition of initial back-arc basin igneous activity.

Do arc and back-arc basin igneous activity coexist?

Results of DSDP Leg 59 led to the hypothesis that Mariana Arc volcanic activity was extinguished for several millions of years during early back-arc basin formation (Scott & Kroenke, 1980; Crawford *et al.*, 1981). This conclusion was criticized by Karig (1983). Cambray *et al.* (1995) suggested that back-arc rifting is associated with intense arc volcanism, but that arc volcanism ceases as spreading is established. Recent Ocean Drilling Program (ODP) drilling in the Lau Basin suggests a 2 my hiatus in arc volcanism as rifting proceeded, with true arc volcanism re-established at ~3·0 Ma (Clift *et al.*, 1995). The early extensional history inferred for the Lau Basin involves cessation of arc volcanism followed by bimodal igneous activity within the embryonic back-arc basin. The arc is re-established at about the same time that seafloor spreading begins.

Because there is no consensus regarding whether or not arc and back-arc basin igneous activity is synchronous or mutually exclusive, valuable insights can be gained from considering active back-arc basin systems. Simultaneous active arc volcanism and seafloor spreading are common for modern arc–back-arc basin systems such as the Mariana and Lau–Tonga systems. There is no a priori reason why arc and back-arc basin magmatic systems should not be able to coexist, where the loci of these magmatic systems are separated by some distance, perhaps 50–100 km or more. Separation of magmatic systems is required because the different magmagenetic styles for arc and Spread BABB are associated with distinct mantle flow regimes. Specifically, most arc melts result from combined deep (~60 km) flux melting and adiabatic decompression during diapiric ascent (Pearce & Peate, 1995), whereas Spread BABB result from MORB-like decompression melting of upwelling mantle (Gribble *et al.*, 1996). However, it is not apparent what happens at the earliest stages of extension, as the arc is rifted and the loci of arc and back-arc basin volcanism are much closer. We question how separate arc and back-arc basin magmagenetic systems could coexist in this situation. Our studies demonstrate that lavas of the Mariana NVTZ are chemically and isotopically indistinguishable from those of the Mariana Arc. We conclude from this, and from the fact that the active arc for ~200 km adjacent to the NVTZ between Nikko and Fukujin is extinct (Bloomer *et al.*, 1989*b*), that the arc magmatic budget has been captured by the rift, that is, diverted to erupt along the extensional axis. This suggests that normal processes of arc melt generation are not

disrupted by incipient rifting. Given that initial rifting involves the lithosphere whereas arc magmas manifest flux melting at depth, the a priori expectation is that arc magmas will continue to be produced regardless of the state of stress in the overlying lithosphere.

In spite of the fact that arc melts should continue to be generated and to erupt thoughout the early stages of rifting, surface manifestations should be affected: an important effect is that volcanism will probably be submarine, because of subsidence associated with crustal thinning. Martinez *et al.* (1995) noted that the pattern of along-strike grabens separated by tectonically disrupted volcanoes is characteristic of early back-arc basin formation. Growth of the large central volcanoes characteristic of mature arcs is unlikely to occur until the arc magma supply is no longer diverted to the extension axis, and this in turn requires migration of the rift axis away from the arc magma supply. This migration corresponds to the rift 'localization' process ascribed by Martinez *et al.* (1995) to the SVTZ. Fukujin is the northernmost active Mariana Arc volcano and lies 30–40 km east of the northernmost SVTZ. We infer that Fukujin is the youngest unequivocal expression of arc re-initiation following rifting. Submarine arc volcanoes extend for 200 km southeast of Fukujin before the first subaerial volcano, Uracas, is encountered. We infer that this distance reflects the greater time that southern volcanoes have had to grow since northward-propagating rifting disrupted the arc. The northern Mariana Trough thus provides confirmation of the inference by Hussong & Uyeda (1981) that Mariana Arc volcanism has been continuous since the Eocene, but that volcanic activity during rifting was submarine, limiting the dispersal of tephra.

The along-strike variations observed for the northern Mariana Trough provide a paradigm for changing styles of arc magmatism in an evolving back-arc basin. First, initial rifting along or near the arc axis disrupts construction of arc edifices because the arc magma supply is diverted to the rift axis. Second, continued extension localizes the rift axis basinward, away from the normal locus of arc volcanism, permitting the re-establishment of the line of arc volcanoes. Finally, arc volcanoes grow above sea-level. Volcanic rocks and associated sediments associated with this evolution can be expected to change with time. We emphasize that, although arc magma supply is continuous, there may be a hiatus in products of subaerial eruptions (such as ash-fall tephra) of as much as a few million years.

Variations in melt generation processes along the extensional axis

A basic tenet of basalt petrogenesis is that incompatible element concentrations are functionally related to the degree of mantle melting. The simplest expression of this relationship is that concentrations of incompatible elements vary inversely with degree of melting (F). Thus, for closed systems, the greater the degree of melting, the lower the concentration of incompatible elements in the melt. The BABB paradox, addressed by Gribble *et al.* (1996), is that for MTB and other BABB, the abundance of some incompatible elements (LILE and fluid-mobile elements) varies directly rather than inversely with F. This represents a significant departure from the standard basalt petrogenetic model. Similar relationships found for arc lavas are inferred to result from introduction of hydrous fluids beneath the arc that lower the temperature of melting and also enrich the mantle in incompatible elements. This process has been called 'flux melting' (Gill, 1981) and is fundamentally an open-system process. Flux melting contrasts with decompression melting, which approximates a closed-system process. The two end-member processes can combine so that hydrous mantle diapirs may melt to a greater extent than would occur as a result of either process alone, and this combination is likely to be important beneath arcs and back-arc basins.

Reasonable estimates of F must be derived before contrasting the trace element behavior of spreading BABB and VTZ basalts. Flat HREE patterns (Fig. 6) indicate that the mantle melting was not associated with residual garnet, which may indicate that melting took place at depths shallower than the stability field of garnet lherzolite (with the possible exception of 48:3-1 and 48:1-3). In this case, F should vary inversely with HREE concentrations. We used abundances of Yb and TiO_2 to quantify F for the NMT. These elements were chosen because addition of slab-derived fluids to the mantle source should have little effect on HFSE such as Ti and Yb (Keppler, 1996). A simple forward model of non-modal batch melting $\{C_O = C_L[D_O + F(1 - P)]$; Shaw, 1970, where C_O is the source composition, prior to melting; C_L is the melt composition, after olivine-only fractionation correction; D_O is the modal bulk coefficient; and P is the non-modal bulk partition coefficient$\}$ of spinel lherzolite is shown as a trajectory superimposed on olivine-only fractionation-corrected samples in Fig. 11. The NMT suite plot on the calculated melt trajectory. Fractionation of other possible phases (i.e. plagioclase and clinopyroxene; magnetite is not likely to precipitate in the basalts studied there) has not been modeled. Fractionation of plagioclase or clinopyroxene can significantly affect Ti and/or Yb contents, so the model presented in Fig. 11 only approximates F. However, only the relative order of degree of melting within the data set is required for the arguments listed below to be valid. Sinton & Fryer (1987) proposed that plagioclase joins olivine on the liquidus in MTB-18 magmas at *mg*-number = 63 (all Fe as Fe^{2+}). Before fractionation correction, the samples plotted in Fig. 11 have *mg*-number >65, except for NVTZ data, which

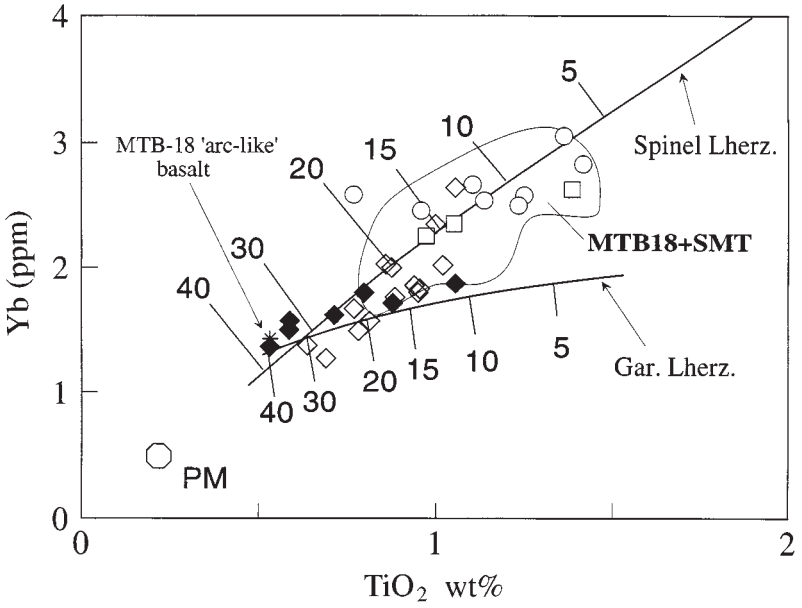

Fig. 11. Estimate of degree of melting, *F*, from Ti–Yb systematics. Glasses with *mg*-number >65 have been corrected for olivine-only fractionation to be in equilibrium with Fo_{90} [K_d(ol) = 0·015, 0·023 for TiO_2 and Yb, respectively]. The curve labeled 'spinel lherz.' is for non-modal batch melting and is labeled with degrees of *F* for 'primitive mantle' (PM) source concentrations of 0·217% TiO_2 and 0·493 ppm Yb (Sun & McDonough, 1989), D_O = 0·117 and 0·127 for a lherzolite composition ol:opx:cpx of 54:30:16, and *P* = 0·325 and 0·397 for ol:opx:cpx melting proportions of 0:30:70. The curve labeled 'Gar. Lherz.' is for non-modal batch melting of a garnet lherzolite 'primitive mantle' source with ol: opx:cpx:gar composition and melt proportion of 52:29:16:3 and 0:45:45:10, respectively. D_O and *P* are 0·127 and 0·247 for TiO_2, and 0·288 and 0·684 for Yb. Both curves are labeled for from 5 to 40% melting. Symbols as in Fig. 3; MTB-22 data of Stern *et al.* (1990) are included with SVTZ data set. Field labeled 'MTB18 + SMT' is the field defined for spreading BABB after Gribble *et al.* (1996). (Note the good correlation between the model spinel lherzolite melting trajectory and NMT data; also note the general increase in *F* to the north.)

include samples with an *mg*-number as low as 47. The errors involved in ignoring fractionation of clinopyroxene and plagioclase from NVTZ compositions are further discussed below.

This model yields estimates for *F* (average of the TiO_2 and Yb estimates) consistent with inferences from bathymetry and other geochemical considerations for Spread BABB. The first-order variations in ridge depth along the spreading BAB are most simply interpreted to result from different degrees of melting, as argued for mid-ocean spreading ridges (Klein & Langmuir, 1987) and the SMT (Gribble *et al.*, 1996). The total range of *F* for Spread BABB is 6–24% (excluding the unusual 'arc-like' sample at MTB-18), and this is also the approximate range proposed for MORB (Klein & Langmuir, 1987). For the 'arc-like' glass (A 1846-9), *F* was determined by using the TiO_2 and Y values listed by Hawkins *et al.* (1990) and the correlation of Y with Yb in MORB [inferred from a Mariana Trough data set with both Y and Yb analyses; Hawkins *et al.* (1990) and references therein]. The *F* = 0·36 calculated here is in good agreement with *F* = 0·34 calculated by Hawkins *et al.* (1990) based on consideration of Ta and Zr systematics. A similar comparison can be made for sample A 1841-11, for which Hawkins *et al.* (1990) calculated *F* = 0·12 and for which our procedure yields *F* = 0·11.

A qualitative check on estimates of *F* is to compare the *F*(TiO_2–Yb) model with an independent function of *F* such as $Na_{8·0}$ [the content of Na_2O at 8% MgO, calculated using the algorithm of Klein & Langmuir (1987)]. Klein & Langmuir (1987) noted that higher average degrees of melting correlate simply with lower sodium content. In Fig. 12, the Ti–Yb model for *F* is compared with $Na_{8·0}$ in which sodium contents are corrected for fractionation (a three-phase, low-pressure assemblage) to 8 wt % MgO to facilitate comparison with the global MORB data set. There is a good correlation of decreasing $Na_{8·0}$ with increasing *F*(TiO_2–Yb) for our NMT data, as well as other samples from the Mariana Trough. Three of the NVTZ samples have MgO < 5% and relatively sodic plagioclase may be involved in their fractionation. However, the sample with the highest *F* (50:1-5) has 6·3 wt % MgO so that the correction to MgO = 8 wt % should not grossly underestimate the sodium content.

Based on consideration of Ti–Yb systematics, the field for Mariana Trough Spread BABB thus records *F* in the range of 6–24% (excepting A 1846-9), yielding a mean of 13 ± 5% (1 SD). This agrees with the range for MTB-18 of 9–17% estimated by Hawkins *et al.* (1990) and 5–19% inferred by Stolper & Newman (1994), and is similar to the range of 8–20% estimated for MORB

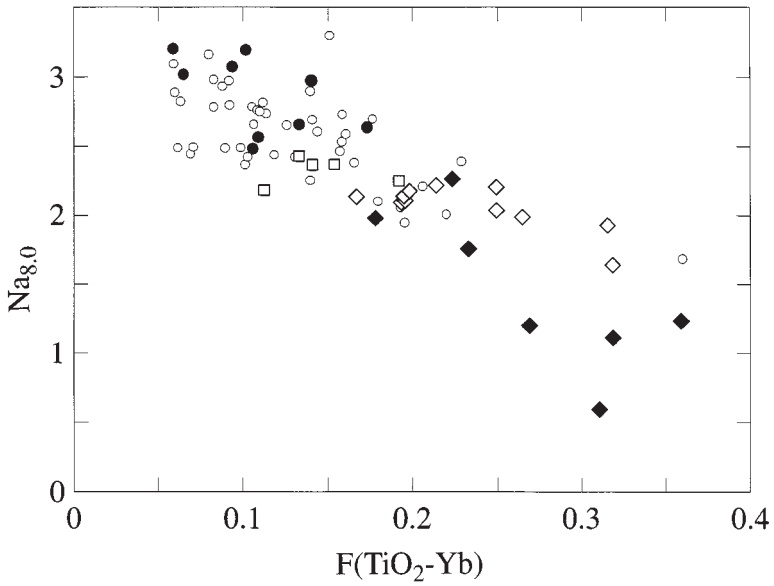

Fig. 12. Comparison of *F* values derived from Ti–Yb systematics (Fig. 11) with Na_2O contents corrected to MgO = 8 wt % by the algorithm of Klein & Langmuir (1987). Symbols as in Fig. 3 except for small circles, which are data for other spreading BABB samples collected south of the study area; filled circles are for SR. (Note the good negative correlation between $Na_{8\cdot0}$ and degree of melting inferred from Ti–Yb systematics. Note that only samples with *mg*-number >62 are plotted.)

(Klein & Langmuir, 1987). A similar extent of melting is inferred for the five CG samples (F = 11–19%, mean 15%). Estimates of F for VTZ lavas are significantly higher than for Spread BABB: F for SVTZ is 23 ± 5% and F for NVTZ is 28 ± 8%). These estimates extend to the high degree of melting (~25%) ascribed to arc basalts from intra-oceanic arcs (Plank & Langmuir, 1988; Pearce & Parkinson, 1993). As discussed above, correction for fractionation of mineral phases other than olivine was not modeled, and fractionation of pyroxene and/or plagioclase complicates estimates of F from Ti–Yb relations. Both pyroxene and plagioclase are common phenocrysts in NVTZ lavas. Uncorrected fractionation of plagioclase decreases the calculated degrees of melting, as (1) plagioclase K_d values for Ti and Yb are $\ll 1$, and (2) the calculated amount of crystal fractionation is a function of *mg*-number only. That is, if there was plagioclase fractionation in addition to olivine, our model will have underestimated F. The effects of uncorrected pyroxene fractionation are more complicated, because pyroxenes have crystal/liquid K_d(Fe/Mg) values that are similar to those of olivine, but are higher for Ti and Yb. Fortunately, pyroxene fractionation is limited for primitive basaltic compositions such as those studied here, and the problem of uncorrected pyroxene fractionation for our estimates of F is likely to be minor. This conclusion is supported by the correspondence between estimates of F for the present sample suite based on Ti–Yb relationships and those obtained by the algorithm of Stolper & Newman (1994).

The normative compositional variations of primitive basalts (*mg*-number >65) indicate that within-suite variations result from variable degrees of melting at moderate to low average pressures with respect to polybaric melting models. Suites with high *mg*-number members form arrays nearly parallel to 1 atm cotectics yet have very narrow ranges in *mg*-number [dredges 46 (*mg*-number = 65–68), 47 (66–69), 48 (66–70), and 68(63–65)] so that it is unlikely that within-suite trends are produced solely by crystal fractionation. This is also shown by the lack of correlation of *mg*-number with the expected fractionation vectors in phase diagrams.

Figure 13 shows the strong increase in F to the north along the extension axis. One possible explanation for this increase would be a lengthened adiabatic decompression path. The dominant control on ascent path length was thought by Plank & Langmuir (1988) to be crustal thickness. Thin crust is expected to underlie the extension axis, with normal oceanic thicknesses (~5–6 km; Bibee *et al.*, 1980) along the spreading ridge and thicker crust (~25 km; Ishihara & Yamazaki, 1991) beneath the NVTZ. If variable lengths of adiabatic ascent along the extension axis were responsible for variations in F, one would expect lower degrees of melting to be associated with the VTZ. Clearly this is not the case.

There are indications that water contents are important for controlling the degree of melting at convergent

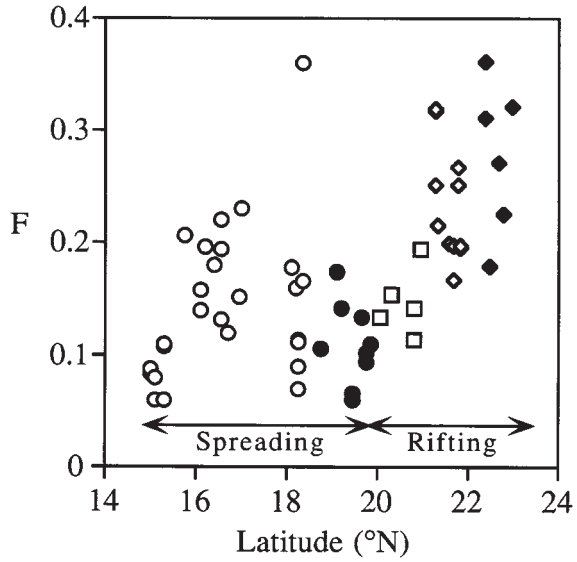

Fig. 13. Extent of melting, *F*, vs latitude in the Mariana Trough back-arc basin. Symbols are as in Fig. 3 except closed symbols are Spreading Ridge data and open symbols are SMT data of Gribble *et al.* (1996) or MTB-18 data of Hawkins *et al.* (1990). Some of the SVTZ data points are data of Stern *et al.* (1990) for which *F* is calculated using our procedure. The significantly greater *F* inferred for SVTZ and NVTZ relative to spreading BABB and Central Graben basalts should be noted.

margins (Davies & Bickle, 1991; Baker *et al.*, 1994). Pearce & Parkinson (1993) inferred that arc melts reflect degrees of melting that range from 15% (thick lithosphere) to 30% (thin lithosphere), of which ~10% melting results from lowering of the liquidus because of addition of water to the mantle and the remainder of the melting is due to decompression. We plot our estimate of melt fraction against source water content (inferred from percent H_2O in sample × $F(TiO_2$–Yb) in Fig. 14. Stolper & Newman (1994) reported a good correlation among MTB-18 samples for *F* (inferred from major element and water data) and weight percent water in the source. Their relationship can be rewritten as $F = 0{\cdot}56W + 0{\cdot}05$, where *F* is the melt fraction and *W* is percent water in the source. Our data allow an assessment of the relationship between *F* and water in the source, indicating $F = 0{\cdot}44W + 0{\cdot}07$. We recognize that Fig. 14 does not plot independent variables (source H_2O is the product of *F* inferred from Ti–Yb systematics and H_2O contents of glass). However, considering that different procedures were used to infer *F* and that only two MTB-18 samples were used for both regressions, the agreement between these two results is very good. Although our VTZ data set is limited (because of a scarcity of glassy, primitive basalts), this regression seems to apply to these as well as spreading BABB. We conclude that there is a relationship in back-arc basin magmagenesis between water in the source and extent of melting, such that quadrupling the water content leads to doubling of the degree of melting. As noted by Plank & Langmuir (1988), this complicates but does not refute models of adiabatic decompression, particularly if source water contents are similar among global arc sysems.

What is the composition of lavas erupted during the early stages of back-arc basin formation?

As outlined in the Introduction, this is a controversial but important subject. This problem should be tackled by considering BAB which have evolved in oceanic settings, because the likely anatexis of continental crust or thick sequences of continental shelf sediments introduces additional complexities (e.g. Sea of Japan, Okinawa Trough, Bransfield Strait). Stern *et al.* (1988) suggested that shoshonitic melts characterized arc regeneration following initial BAB rifting, but the tectonic studies of Martinez *et al.* (1995) and Baker *et al.* (1996) have since demonstrated that the region defined by the Alkalic Volcanic Province (Bloomer *et al.*, 1989*a*) occupies a 'pre-rift' position. Crawford *et al.* (1981) inferred an early boninitic phase, but such lavas probably only erupt where BAB extension axes intersect a forearc, such as at the northernmost Tonga arc (Falloon & Crawford, 1991). Early lavas that are MORB-like have been reported for the Lau Basin (Hawkins, 1995), and early rift stages for this system represented by the southern Havre Trough and Ngatoro Rift erupt both arc-like and MORB-like lavas (Gamble & Wright, 1995). Recent investigations of the Sumisu Rift in the Bonin Arc, which is in the early stages of back-arc basin evolution, have led to the

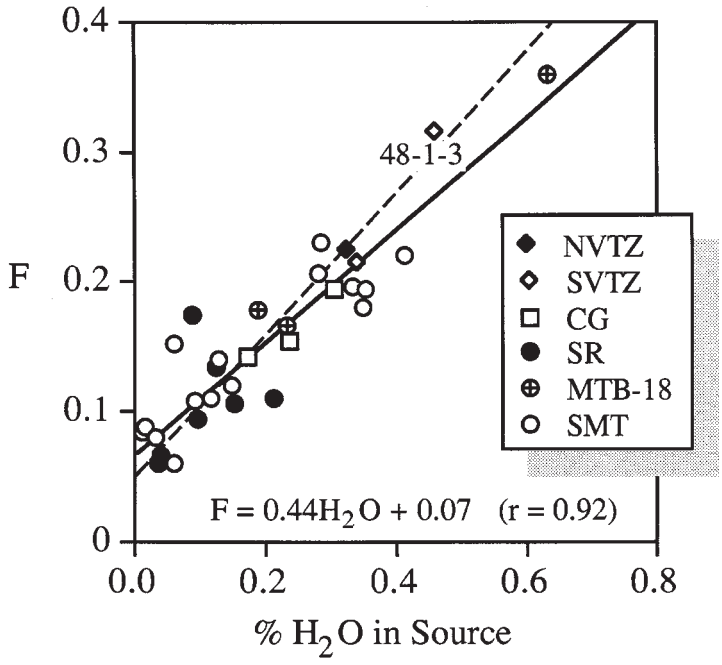

Fig. 14. Extent of melting, *F*, vs percent water in the source. Water content of the source is inferred to be equal to percent H_2O in sample × *F*(TiO_2–Yb). (Note that sample 48-1-3 may have degassed water, so inferred source water content for this sample is a minimum estimate.) Regression excludes sample 48:1-3. Continuous line corresponds to the regression preferred here ($F = 0{\cdot}44H_2O + 0{\cdot}07$; $r = 0{\cdot}92$). Dashed line is the regression of Stolper & Newman (1994), which can be rewritten as $F = 0{\cdot}56H_2O + 0{\cdot}05$.

conclusion that typical BABB are erupted from the earliest stages (Fryer *et al.*, 1990). It should be noted that rift stages reflected by the Sumisu Rift and the northern Mariana Trough are distinct in several ways: (1) rifting has not disrupted the magmatic arc east of the Sumisu Rift but has in the NMT; (2) Sumisu Rift volcanism is concentrated along a NE-trending alignment that lies at high angles to the extension axis (Smith *et al.*, 1990), whereas NMT volcanic activity is concentrated along the extension axis (Martinez *et al.*, 1995; Baker *et al.*, 1996); (3) arc lavas in the vicinity of the Sumisu Rift are depleted tholeiites, similar in many respects to BABB. Many of the compositional differences between these arc lavas and those of the Sumisu Rift proper can be related to decreased degrees of melting for Sumisu Rift lavas relative to the arc as a function of decreased water flux with distance from the trench. Indeed, much of the controversy about whether or not BABB is produced during the initial stages of back-arc rifting is semantic, and reflects the fact that there are few classification schemes that effectively distinguish Spread BABB from arc basalts. Such distinctions should be made for systems such as the Marianas or Lau–Tonga, where compositional ranges for Spread BABB and arc basalts are recognized, and where the transition from rifting to spreading can be studied.

We have demonstrated that, for the early rift stage defined by the Mariana Trough NVTZ, the extension axis has captured the arc magmatic budget. Lavas erupting from this part of the rift cannot be compositionally distinguished from Mariana Arc lavas, and this argues for similar petrogenetic processes. This is consistent with what we understand about the petrogenesis of back-arc basin basalts. Spread BABB results from the interaction of a subduction component and processes of adiabatic decompression that are indistinguishable from those operating beneath mid-ocean ridges (Gribble *et al.*, 1996). In this case, analogy with events accompanying continental rifting progressing to seafloor spreading would indicate that substantial extension ($\beta \sim 5$; White & McKenzie, 1989) is necessary before induced mantle upwelling is sufficient to generate Spread BABB. From this perspective, it is impossible to generate Spread BABB during the earliest stages of BAB rifting. Assuming that Spread BABB are now erupting ~400 km south of the tip of propagating rifting and that rifting and spreading are propagating northward at 100–400 mm/my (Martinez *et al.*, 1995), eruption of Spread BABB followed rift initiation by 1–4 my.

These ideas are schematically demonstrated in Fig. 15. Flow of mantle beneath the arc is normally subhorizontal and towards the trench in the shallow asthenosphere and

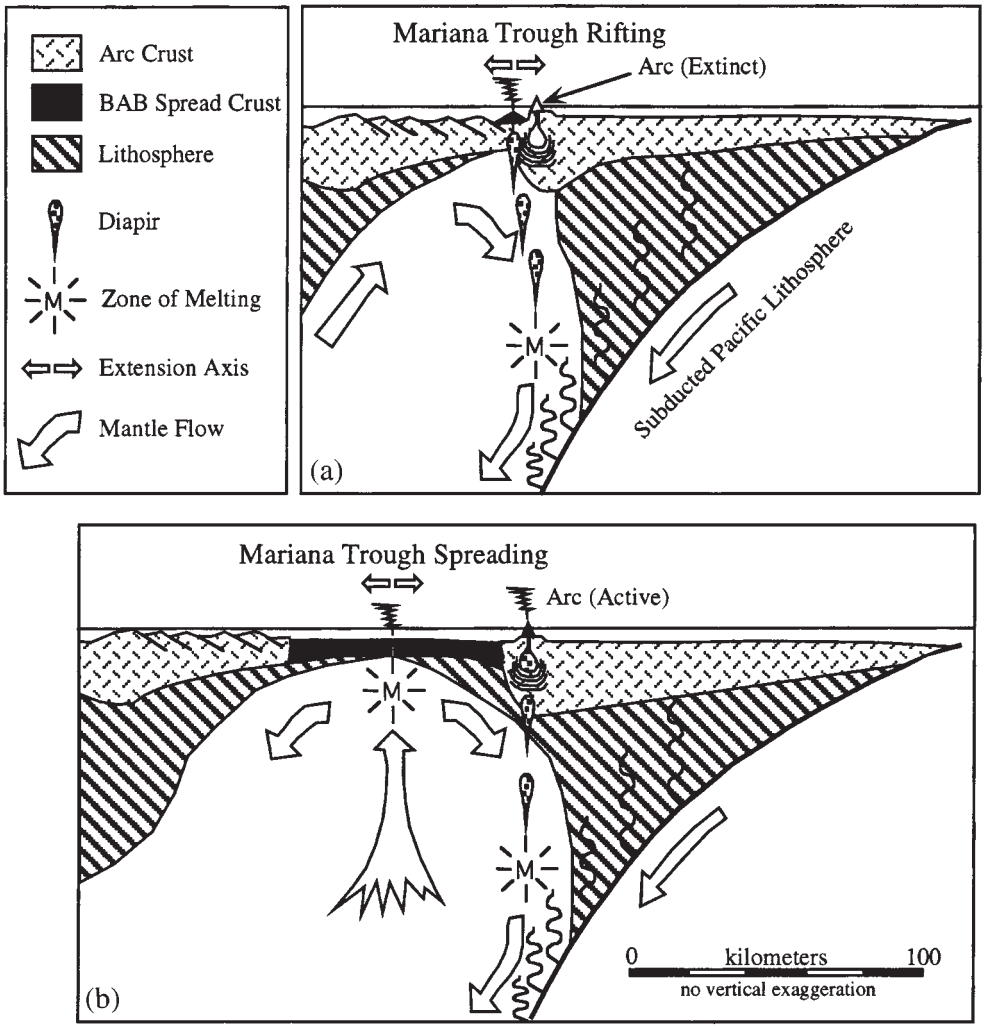

Fig. 15. Schematic representation of tectonics showing changing patterns of mantle convection and processes of melt generation associated with an evolving back-arc basin such as the Mariana Trough. (a) Early rifting does not perturb normal processes of arc magmagenesis in the mantle. Arc melts result from the rise of buoyant diapirs at a rate that allows these to overcome the ambient mantle downflow induced by the subducting slab. These melts are diverted from the arc to the nearby rift axis, where the intersection of point source magma supply with 2-D rift crustal structures results in volcanic styles of the VTZ. (b) Establishment of a seafloor spreading regime reflects establishment of a zone of mantle upwelling beneath the spreading ridge, resulting in decompression melting of a nearly adiabatic mantle column indistinguishable from that of normal mid-ocean ridges. Arc magmas continue to be generated in association with diapiric ascent against ambient downward mantle flow, but the separation of extension axis and the arc volcanic front allows development of a normal magmatic arc.

downward, away from the arc in the deeper asthenosphere (Davies & Stevenson, 1992). Arc magmas may ascend diapirically through the mantle flow (Davies & Stevenson, 1992), in contrast to the situation beneath mid-ocean ridges where decompression melting occurs as mantle flow is focused beneath the ridge (Spiegelman & McKenzie, 1987). The early stages of extension are not likely to affect deep processes of mantle convection, metasomatism, and melting: these occur at depths of 70 km or more. Whereas arc melt generation continues unabated during rifting, extension does affect the surficial expression of arc volcanism, because diapirs and their melts are diverted to the nearby extension axis. This can also affect the amount of melting caused by adiabatic decompression, which should increase as the crust thins (Plank & Langmuir, 1988). Figure 15a approximates the tectono-magmatic situation of the earliest stages in BAB formation, as typified by the Mariana Trough NVTZ. It is impossible to organize the mantle upwelling required to generate MORB-like decompression melts as long as induced mantle downwelling persists beneath the extension axis. With continued extension, the rift axis moves away from what would be the arc magmatic front, and progressively less of the arc magmatic flux is diverted to

the extension axis as the basin widens. The magmatic arc is rebuilt near the trenchward margin of the rifted arc crust. This is the situation for the Mariana Trough SVTZ. As extension continues, the rift axis becomes progressively more distant from the arc magmatic flux and may undergo amagmatic extension: this may be the cause of the Central Graben. Finally, the distance between the axis of extension and the zone of sub-arc mantle downwelling is sufficient to allow mantle upwelling to become established and generate a mid-ocean ridge-like decompression melting system, as shown in Fig. 15b. Seafloor spreading is established at this time and will continue as long as appropriate stresses are applied, although the degree of melting is likely to diminish as the zone of upwelling is progressively separated from sources of slab-derived water.

CONCLUSIONS

The magmatic expression of the earliest stages in the formation of back-arc basins involves unique interactions between downward-flowing mantle, ascending diapirs of arc melt, and evolving lithospheric strain regimes. Fresh lavas collected from along the extension axis of the northern Mariana Trough reveal systematic variations in source compositions and magmagenetic styles that provide a first look at the spectrum of products associated with variations in extension from incipient rifting to seafloor spreading. These samples reveal systematic changes in magma chemical and isotopic compositions that manifest a progressive transition, from early rift lavas that are indistinguishable from arc lavas to basalts produced by decompression melting resulting from mantle upwelling beneath back-arc basin spreading centers. This transition reflects a reorganization of mantle convective regimes beneath evolving back-arc basins, from lateral flow or downwelling beneath incipient rifts to upwelling beneath zones of seafloor spreading. The most important change that happens in arc and back-arc basin magmatic systems as back-arc basins evolve is not the termination of arc igneous activity, because arc magmas are constantly being generated deep in the mantle wedge. The most important change in the case of the Mariana Arc system is the establishment, 1–4 my after rift initiation, of an independent magmatic system in the back-arc basin and seafloor spreading. Future research should focus on development of physical models for how this reorganization is accomplished, how this transition affects magmagenesis beneath youthful back-arc basins, and what communication occurs between upwelling mantle and downwelling mantle.

ACKNOWLEDGEMENTS

We thank the Captain and the crew of the R.V. *Thomas Washington*. This research was supported by NSF grants to R. J. S. and S. H. B. Special thanks are due to Drs Jongman Lee and Mohamed Gamal Abdelsalam for analytical assistance. We thank also James F. Allan and two anonymous referees for their helpful comments and criticisms. This is UTD Geosciences Contribution 869.

REFERENCES

Baker, M. B., Grove, T. L. & Price, R., (1994). Primitive basalts and andesites from the Mt. Shasta region, N. California: products of varying melt fraction and water content. *Contributions to Mineralogy and Petrology* **118,** 111–129.

Baker, N., Fryer, P., Martinez, F. & Yamazaki, T., (1996). Rifting history of the Northern Mariana Trough: SeaMARC II and Seismic Reflection surveys. *Journal of Geophysical Research* **101**(B5), 11427–11455.

Beard, J. S., (1995). Experimental, geological and geochemical constraints on the origins of low-K silicic magmas in oceanic arcs. *Journal of Geophysical Research* **100,** 15593–15600.

Bibee, L. D., Shor, G. G., Jr & Lu, R. S., (1980). Inter-arc spreading in the Mariana Trough. *Marine Geology* **35,** 183–197.

Bloomer, S. H., Stern, R. J., Fisk, E. & Geschwind, C. H., (1989*a*). Shoshonitic volcanism in the Northern Mariana Arc 1. Mineralogic and major and trace element characteristics. *Journal of Geophysical Research* **94,** 4469–4496.

Bloomer, S. H., Stern, R. J. & Smoot, N. C., (1989*b*). Physical volcanology of the submarine Mariana and Volcano Arcs. *Bulletin of Volcanology* **51,** 210–224.

Cambray, H., Publlier, M., Jolivet, L. & Pouclet, A., (1995). Volcanic activity recorded in deep-sea sediments and the geodynamic evolution of western Pacific island arcs. In: Taylor, B. & Natland, J. (eds) *Active Margins and Marginal Basins of the Western Pacific. Geophysical Monograph, American Geophysical Union* **88,** 97–124.

Clift, P. D., (1995). Volcaniclastic sedimentation and volcanism during the rifting of Western Pacific backarc basins. In: Taylor, B. & Natland, J. (eds) *Active Margins and Marginal Basins of the Western Pacific. Geophysical Monograph, American Geophysical Union* **88,** 67–96.

Clift, P. D. & ODP Leg 135 Scientific Party, (1995). Volcanism and sedimentation in a rifting island-arc terrain: an example from Tonga, SW Pacific. In: Smellie, J. L. (ed.) *Volcanism Associated with Extension at Consuming Plate Margins. Geological Society, London, Special Publication* **81,** 29–51.

Crawford, A. J., Beccaluva, L. & Serri, G., (1981). Tectono-magmatic evolution of the West Philippine–Mariana region and the origin of boninites. *Earth and Planetary Science Letters* **54,** 346–356.

Danyushevsky, L. V., Falloon, T. J., Sobolev, A. V., Crawford, A. J., Carroll, M. & Price, R. C., (1993). The H_2O content of basalt glasses from Southwest Pacific back-arc basins. *Earth and Planetary Science Letters* **117,** 347–362.

Davies, J. H. & Bickle, M. J., (1991). A physical model for the volume and composition of melt produced by hydrous fluxing above subduction zones. *Philosophical Transactions of the Royal Society of London, Series A* **335,** 355–364.

Davies, J. H. & Stevenson, D. J., (1992). Physical model of source region of subduction volcanics. *Journal of Geophysical Research* **97,** 2037–2070.

Dixon, J. E., Stolper, E. M. & Delaney, J. R., (1988). Infrared spectroscopic measurement of CO_2 and H_2O in Juan de Fuca Ridge basaltic glasses. *Earth and Planetary Science Letters* **90,** 97–104.

Dixon, J. E., Clague, D. A. & Stolper, E. M., (1991). Degassing history of water, sulfur, and carbon in submarine lavas from Kilauea Volcano, Hawaii. *Journal of Geology* **99,** 371–394.

Dixon, J. E., Stolper, E. M. & Holloway, J. R., (1995). An experimental study of water and carbon dioxide solubilities in mid-ocean ridge basaltic liquids. Part I: Calibration and solubility models. *Journal of Petrology* **36,** 1607–1631.

Eguchi, T., (1984). Seismotectonics around the Mariana Trough. *Tectonophysics* **102,** 33–52.

Falloon, T. J. & Crawford, A. J., (1991). The petrogenesis of high-calcium boninite lavas dredged from the northern Tonga ridge. *Earth and Planetary Science Letters* **102,** 375–394.

Forsyth, D. W., (1992). Geophysical constraints on mantle flow and melt generation beneath mid-ocean ridges. In: Morgan, J. P., Blackman, D. K. & Sinton, J. M. (eds) *Mantle Flow and Melt Generation at Mid-Ocean Ridges. Geophysical Monograph, American Geophysical Union* **71,** 1–65.

Fryer, P., Sinton, J. M. & Philpotts, J. A., (1981). Basaltic glasses from the Mariana Trough. *Initial Reports of the Deep Sea Drilling Project, 60*. Washington, DC: US Government Printing Office, pp. 601–609.

Fryer, P., Taylor, B., Langmuir, C. H. & Hochstaedter, A. G., (1990). Petrology and geochemistry of lavas from the Sumisu and Torishima backarc rifts. *Earth and Planetary Science Letters* **100,** 161–178.

Gamble, J. A. & Wright, I. C., (1995). The Southern Havre Trough: geological structure and magma petrogenesis of an active backarc rift complex. In: Taylor, B. (ed.) *Backarc Basins: Tectonics and Magmatism*. New York: Plenum, pp. 29–62.

Garcia, M. O., Liu, N. W. K. & Muenow, D. W., (1979). Volatiles in submarine volcanic rocks from the Mariana Island arc and trough. *Geochimica et Cosmochimica Acta* **43,** 305–312.

Gill, J., (1981). *Orogenic Andesites and Plate Tectonics*. New York: Springer-Verlag.

Gribble, R. F., Stern, R. J., Bloomer, S. H., Stuben, D., O'Hearn, T. & Newman, S., (1996). MORB mantle and subduction components interact to generate basalts in the Southern Mariana Trough back-arc basin. *Geochimica et Cosmochimica Acta* **60,** 2153–2166.

Hart, S. R., (1984). A large-scale isotope anomaly in the southern hemisphere mantle. *Nature* **309,** 753–757.

Hart, S. R., Glassley, W. E. & Karig, D. E., (1972). Basalts and sea floor spreading behind the Mariana Island Arc. *Earth and Planetary Science Letters* **15,** 12–18.

Hawkins, J. W., (1995). Evolution of the Lau Basin—insights from ODP Leg 135. In: Taylor, B. & Natland, J. (eds) *Active Margins and Marginal Basins of the Western Pacific. Geophysical Monograph, American Geophysical Union* **88,** 125–173.

Hawkins, J. W. & Melchior, J. T., (1985). Petrology of Mariana Trough and Lau Basin basalts. *Journal of Geophysical Research* **90,** 11431–11468.

Hawkins, J. W., Bloomer, S. H., Evans, C. A. & Melchior, J. T., (1984). Evolution of intra-oceanic arc–trench systems. *Tectonophysics* **102,** 175–205.

Hawkins, J. W., Macdougall, J. D. & Volpe, A. M., (1990). Petrology of the axial ridge of the Mariana Trough backarc spreading center. *Earth and Planetary Science Letters* **100,** 226–250.

Hickey-Vargas, R., (1991). Isotope characteristics of submarine lavas from the Philippine Sea: implications for the origin of arc and basin magmas of the Philippine tectonic plate. *Earth and Planetary Science Letters* **107,** 290–304.

Hofmann, A. W., (1988). Chemical differentiation of the Earth: the relationship between mantle, continental crust, and oceanic crust. *Earth and Planetary Science Letters* **90,** 297–314.

Hussong, D. M. & Uyeda, S., (1981). Tectonic processes and the history of the Mariana Arc: a synthesis of the results of Deep Sea Drilling Project leg 60. *Initial Reports of the Deep Sea Drilling Project, 60*. Washington, DC: US Government Printing Office, pp. 909–929.

Ishihara, T. & Yamazaki, T., (1991). Gravity anomalies over the Izu–Ogasawara (Bonin) and northern Mariana arcs. *Bulletin of the Geological Survey of Japan* **42,** 687–701.

Jackson, M. C., (1989). Petrology and petrogenesis of recent submarine volcanics from the northern Mariana Arc and back-arc basin. Ph.D. Dissertation, University of Hawaii, Honolulu.

Karig, D. E., (1971). Origin and development of marginal basins in the western Pacific. *Journal of Geophysical Research* **76,** 2542–2561.

Karig, D. E., (1983). Temporal relationships between back arc basin formation and arc volcanism with special reference to the Philippine Sea. In: Hayes, D. (ed.) *The Tectonic and Geologic Evolution of Southeast Asian Seas and Islands, Part 2. Geophysical Monograph, American Geophysical Union* **27,** 318–325.

Katsumata, M. & Sykes, L. R., (1969). Seismicity and tectonics of the western Pacific: Izu–Mariana–Caroline and Ryukyu–Taiwan regions. *Journal of Geophysical Research* **74,** 5923–5948.

Keppler, H., (1996). Constraints from partitioning experiments on the composition of subduction-zone fluids. *Nature* **380,** 237–240.

Kinzler, R. J. & Grove, T. L., (1992). Primary magmas of mid-ocean ridge basalts 2. Applications. *Journal of Geophysical Research* **97,** 6907–6926.

Klein, E. M. & Langmuir, C. H., (1987). Global correlations of ocean ridge basalt chemistry with axial depth and crustal thickness. *Journal of Geophysical Research* **92,** 8089–8115.

Kress, V. C. & Carmichael, I. S. E., (1988). Stoichiometry of the iron oxidation reaction in silicate melts. *American Mineralogist* **73,** 1267–1274.

Lee, J., Stern, R. J. & Bloomer, S. H., (1995). Forty million years of magmatic evolution in the Mariana arc: the tephra glass record. *Journal of Geophysical Research* **100,** 17671–17687.

LeMaitre, R. W., (1989). *A Classification of Igneous Rocks and Glossary of Terms*. Oxford: Blackwell Scientific, 193 pp.

Lin, P.-N., Stern, R. J. & Bloomer, S. H., (1989). Shoshonitic volcanism in the Northern Mariana Arc. 2. Large-ion lithophile and rare earth element abundances evidence for the source of incompatible element enrichments in intraoceanic arcs. *Journal of Geophysical Research* **94,** 4497–4514.

Lonsdale, P. & Hawkins, J., (1985). Silicic volcanism at an off-axis geothermal field in the Mariana Trough back-arc basin. *Geological Society of America Bulletin* **96,** 940–951.

Malinverno, A., (1993). Transition between a valley and a high at the axis of mid-ocean ridges. *Geology* **21,** 639–642.

Manton, W. I., (1988). Separation of Pb from young zircons by single-bead ion exchange. *Chemical Geology* **73,** 147–152.

Marsaglia, K. M., (1995). Interarc and backarc basins. In: Busby, C. J. & Ingersoll, R. V. (eds) *Tectonics of Sedimentary Basins*. Cambridge, MA: Blackwell Science, pp. 299–329.

Martinez, F., Fryer, P., Baker, N. A. & Yamazaki, T., (1995). Evolution of backarc rifting: Mariana Trough, 20°–24°N. *Journal of Geophysical Research* **100,** 3807–3827.

McCulloch, M. T. & Gamble, J. A., (1991). Geochemical and geodynamical constraints on subduction zone magmatism. *Earth and Planetary Science Letters* **102,** 358–374.

Meijer, A., (1976). Pb and Sr isotopic data bearing on the origin of volcanic rocks from the Mariana island-arc system. *Geological Society of America Bulletin* **87,** 1358–1369.

Melson, W. G., Vallier, T. L., Wright, T. L., Byerly, G. & Nelen, J., (1976). Chemical diversity of abyssal volcanic glasses erupted along Pacific, Atlantic and Indian ocean sea-floor spreading centers. In:

Sutton, G. H., Manghnani, M. H., Moberly, R. & McAfee, E. U. (eds) *The Geophysics of the Pacific Ocean Basin and its Margin. Geophysical Monograph, American Geophysical Union* **19,** 351–367.

Park, C., Tamaki, K. & Kobayashi, K., (1990). Age–depth correlation of the Philippine Sea back-arc basins and other marginal basins in the world. *Tectonophysics* **181,** 351–371.

Pearce, J. A. & Parkinson, I. J., (1993). Trace element models for mantle melting: application to volcanic arc petrogenesis. In: Prichard, H. M., Alabaster, T., Harris, N. B. W. & Neary, C. R. (eds) *Magmatic Processes and Plate Tectonics. Geological Society, London, Special Publication* **76,** 373–403.

Pearce, J. A. & Peate, D. W., (1995). Tectonic implications of the composition of volcanic arc magmas. *Annual Review of Earth and Planetary Sciences* **23,** 251–285.

Pier, J. G., Podosek, F. A., Luhr, J. F., Brannon, J. C. & Aranda-Gomez, J. J., (1989). Spinel-lherzolite-bearing Quaternary volcanic centers in San Luis Potosi, Mexico. 2. Sr and Nd isotopic systematics. *Journal of Geophysical Research* **94,** 7941–7951.

Plank, T. & Langmuir, C. H., (1988). An evaluation of the global variations in the major element chemistry of arc basalts. *Earth and Planetary Science Letters* **90,** 349–370.

Richard, P., Shimizu, N. & Allegre, C. J., (1976). $^{143}Nd/^{146}Nd$, a natural tracer. An application to oceanic basalts. *Earth and Planetary Science Letters* **31,** 269–278.

Schmidt, R. G., 1957. Petrology of the volcanic rocks. In *Geology of Saipan, Mariana Islands. US Geological Survey Professional Paper* **280C,** 127–176.

Scott, R. & Kroenke, L., (1980). Evolution of back arc spreading and arc volcanism in the Philippine Sea: interpretation of Leg 59 DSDP results. In: Hayes, D. E. (ed.) *The Tectonic and Geologic Evolution of Southeast Asian Seas and Islands. Geophysical Monograph, American Geophysical Union* **23,** 283–291.

Shaw, D. M., (1970). Trace element fractionation during anatexis. *Geochimica et Cosmochimica Acta* **34,** 237–243.

Shibata, T. & Segawa, K., (1985). Basaltic glasses from the northern Mariana Trough. In: Kobayashi, K. (ed.) *Preliminary Report of the Hakuho Maru Cruise KH84-1*. Tokyo: Ocean Research Institute, University of Tokyo, pp. 214–224.

Sinton, J. M. & Fryer, P., (1987). Mariana Trough lavas from 18°N: implications for the origin of back arc basin basalts. *Journal of Geophysical Research* **92,** 12782–12802.

Smith, J. R., Taylor, B., Malahoff, A. & Petersen, L., (1990). Submarine volcanism in the Sumisu Rift, Izu–Bonin arc: submersible and deep-tow camera results. *Earth and Planetary Science Letters* **100,** 148–160.

Spiegelman, M. & McKenzie, D., (1987). Simple 2-D models for melt extraction at mid-ocean ridges and island arcs. *Earth and Planetary Science Letters* **83,** 137–152.

Stern, R. J., Bloomer, S. H., Lin, P. N., Ito, E. & Morris, J., (1988). Shoshonitic magmas in nascent arcs: new evidence from submarine volcanoes in the northern Marianas. *Geology* **16,** 426–430.

Stern, R. J., Lin, P., Morris, J. D., Jackson, M. C., Fryer, P., Bloomer, S. H. & Ito, E., (1990). Enriched back-arc basin basalts from the northern Mariana Trough: implications for the magmatic evolution of back-arc basins. *Earth and Planetary Science Letters* **100,** 210–225.

Stern, R. J., Jackson, M. C., Fryer, P. & Ito, E., (1993). O, Sr, Nd, and Pb isotopic composition of the Kasuga Cross-Chain in the Mariana Arc: a new perspective on the K–h relationship. *Earth and Planetary Science Letters* **119,** 459–475.

Stern, R. J., Bloomer, S. H., Martinez, F., Yamazaki, T. & Harrison, T. M., (1996). The composition of back-arc basin lower crust and upper mantle in the Mariana Trough: a first report. *Island Arc* **5,** 354–372.

Stolper, E. & Newman, S., (1994). The role of water in the petrogenesis of Mariana Trough magmas. *Earth and Planetary Science Letters* **121,** 293–325.

Sun, S.-S. & McDonough, W. F., (1989). Chemical and isotopic systematics of oceanic basalts: implications for mantle composition and processes. In: Saunders, A. D. & Norry, M. J. (eds) *Magmatism in the Ocean Basins. Geological Society, London, Special Publication* **42,** 313–345.

Tatsumi, Y., Otofuji, Y.-I., Matsuda, T. & Nohda, S., (1989). Opening of the Sea of Japan back-arc basin by asthenospheric injection. *Tectonophysics* **166,** 317–329.

Tormey, D. R., Grove, T. L. & Bryan, W. B., (1987). Experimental petrology of normal MORB near the Kane Fracture Zone: 22°–25°N, mid-Atlantic ridge. *Contributions to Mineralogy and Petrology* **96,** 121–139.

Volpe, A. M., Macdougall, J. D. & Hawkins, J. W., (1987). Mariana Trough basalts (MTB): trace element and Sr–Nd isotopic evidence for mixing between MORB-like and arc-like melts. *Earth and Planetary Science Letters* **82,** 241–254.

Volpe, A. M., Macdougall, J. D., Lugmair, G. W., Hawkins, J. W. & Lonsdale, P., (1990). Fine-scale isotopic variation in Mariana Trough basalts: evidence for heterogeneity and a recycled component in backarc basin mantle. *Earth and Planetary Science Letters* **100,** 251–264.

White, R. S. & McKenzie, D. P., (1989). Magmatism at rift zones: the generation of volcanic continental margins and flood basalts. *Journal of Geophysical Research* **94,** 7685–7729.

White, W. M. & Patchett, J., (1984). Hf-Nd-Sr isotopes and element abundances in island arcs: implications for magma origins and crust-mantle evolution. *Earth and Planetary Science Letters* **67,** 167–185.

Wood, D. A., Marsh, N. G., Tarney, J., Joron, J.-L., Fryer, P. & Treuil, M., (1981). Geochemistry of igneous rocks recovered from a transect across the Mariana Trough, Arc, Fore-arc, and Trench, Sites 453 through 461, Deep Sea Drilling Project Leg 60. In: Hussong, D. M., Uyeda, S., *et al.* (eds) *Initial Reports of the Deep Sea Drilling Project, Leg 60*. Washington, DC: US Government Printing Office, pp. 611–645.

Woodhead, J. D. & Fraser, D. G., (1985). Pb, Sr and ^{10}Be isotopic studies of volcanic rocks from the Northern Mariana Islands. Implications for magma genesis and crustal recycling in the Western Pacific. *Geochimica et Cosmochimica Acta* **49,** 1925–1930.

Zindler, A., Jagoutz, E. & Goldstein, S., (1982). Nd, Sr and Pb isotopic systematics in a three-component mantle: a new perspective. *Nature* **58,** 519–523.